

**Geodetic mass
balance record with
rigorous uncertainty
estimates**

E. Magnússon et al.

Geodetic mass balance record with rigorous uncertainty estimates deduced from aerial photographs and LiDAR data – case study from Drangajökull ice cap, NW-Iceland

E. Magnússon¹, J. M. C. Belart¹, F. Pálsson¹, H. Ágústsson², and P. Crochet²

¹Institute of Earth Sciences, University of Iceland, Sturlugata 7, 101 Reykjavik, Iceland

²Icelandic Meteorological Office, Bústaðavegi 7–9, 108 Reykjavik, Iceland

Received: 13 July 2015 – Accepted: 18 August 2015 – Published: 9 September 2015

Correspondence to: E. Magnússon (eyjolm@hi.is)

Published by Copernicus Publications on behalf of the European Geosciences Union.

Title Page

Abstract

Introduction

Conclusions

References

Tables

Figures

◀

▶

◀

▶

Back

Close

Full Screen / Esc

Printer-friendly Version

Interactive Discussion



Abstract

In this paper we describe how recent high resolution Digital Elevation Models (DEMs) can be used as constraints for extracting glacier surface DEMs from old aerial photographs and to evaluate the uncertainty of the mass balance record derived from the DEMs. We present a case study for Drangajökull ice cap, NW-Iceland. This ice cap covered an area of 144 km² when it was surveyed with airborne LiDAR in 2011. Aerial photographs spanning all or most of the ice cap are available from survey flights in 1946, 1960, 1975, 1985, 1994 and 2005. All ground control points used to constrain the orientation of the aerial photographs were obtained from the high resolution LiDAR DEM (2 m × 2 m cell size and vertical accuracy < 0.5 m). The LiDAR DEM was also used to estimate errors of the extracted photogrammetric DEMs in ice and snow free areas, at nunataks and outside the glacier margin. The derived errors of each DEM were used to constrain a spherical variogram model, which along with the derived errors in ice and snow free areas were used as inputs into 1000 Sequential Gaussian Simulations (SGSim). The simulations were used to estimate the possible bias in the entire glaciated part of the DEM. The derived bias correction, varying in magnitude between DEMs from 0.03 to 1.66 m (1946 DEM) was then applied. The simulation results were also used to calculate the 95 % confidence level of this bias, resulting in values between ±0.21 m (in 2005) and ±1.58 m (in 1946). Error estimation methods based on more simple proxies would typically yield 2–4 times larger error estimates. The aerial photographs used were acquired between late June and early October. An additional bias correction was therefore estimated using a degree day model to obtain the volume change between the start of two hydrological years (1 October). This correction corresponds to an average elevation change of ~ -3 m in the worst case for 1960, or about ~ 2/3 of volume change between the 1960 and the 1975 DEMs. The total uncertainty of the derived mass balance record is mostly due to uncertainty of the SGSim bias correction, the uncertainty of the seasonal bias correction and the uncertainty of the interpolated glacier surface where data is lacking. The record shows a glacier-wide

Geodetic mass balance record with rigorous uncertainty estimates

E. Magnússon et al.

Title Page

Abstract

Introduction

Conclusions

References

Tables

Figures



Back

Close

Full Screen / Esc

Printer-friendly Version

Interactive Discussion



**Geodetic mass
balance record with
rigorous uncertainty
estimates**

E. Magnússon et al.

Title Page

Abstract

Introduction

Conclusions

References

Tables

Figures

◀

▶

◀

▶

Back

Close

Full Screen / Esc

Printer-friendly Version

Interactive Discussion



mass balance rate of $\dot{B} = -0.250 \pm 0.040$ m w.e. a^{-1} for the entire study period (1946–2011). We observe significant decadal variability including positive periods, peaking in 1985–1994 with $\dot{B} = 0.26 \pm 0.11$ m w.e. a^{-1} . There is a striking difference if \dot{B} is calculated separately for the western and eastern halves of Drangajökull, with a reduction of eastern part on average ~ 3 times faster than the western part. Our study emphasises the need of applying rigorous geostatistical methods for obtaining uncertainty estimates of geodetic mass balance, the importance of seasonal corrections of DEMs from glaciers with high mass turnover and the risk of extrapolating mass balance record from one glacier to another even over short distances.

1 Introduction

Mountain glaciers and ice caps accounted for more than half of the land ice runoff contribution to global mean sea level rise during the 20th century (Vaughan et al., 2013). Understanding how these glaciers respond to a changing climate is essential to close the budget of sea-level rise over the last decades and project the sea-level rise in the near future. In recent years an increased part of our knowledge on how these glaciers are changing has been based on remote sensing. The majority of these studies describe current or recent glacier changes in different parts of the globe applying geodetic methods (Gardelle et al., 2012; Berthier et al., 2010). Others have presented results on the geodetic mass balance extending further back (e.g. Fischer et al., 2015; Nuth et al., 2007) but these studies are particularly important since they indicate how the glaciers responded to 20th century climate variability. Such observations can be used to constrain or correct glacier mass balance models that are used to estimate how the glaciers will respond to future climate changes (e.g. Clarke et al., 2015).

Studies on long term geodetic mass balance are generally based on digitised contour maps, with some exceptions where mass balance records have been derived from Digital Elevation Models (DEMs) extracted from old archives of aerial photographs applying digital photogrammetry (e.g. James et al., 2012). The applicability of geodetic

mass balance records as a key to predicting future glacier changes depends on the accuracy of such records and their resolution. To maximize both the accuracy and the resolution we should rather focus, if possible, on archives of aerial photographs, because:

- i. These archives often span more epochs than the published topographic maps.
- ii. With new and rapidly improving tools in digital photogrammetry the potential to produce much more accurate and detailed DEMs than those deduced by interpolating elevation contours from old maps has increased significantly.
- iii. The availability of high resolution DEMs has opened a new source of ground control points (GCPs) for constraining the orientation of photogrammetric DEMs (Barrand et al., 2009). Like (ii), this will lead to more accurate DEMs from aerial photograph archives in future studies. New spaceborne sensors such as Worldview and Pléiades may allow such studies in remote areas without conducting expensive field campaigns to survey GCPs.

In order to maximize the value of geodetic mass balance records, realistic uncertainty assessments are required. If the uncertainty is overestimated, the value of the information that we can extract from the geodetic data will be diminished, the results will be neglected by the scientific community or not even be published. If, however, the uncertainty is underestimated, geodetic mass balance records with significant errors will be interpreted as solid observations. When extracting volume change from two different DEMs a common approach is to use the standard deviation of the DEM difference in the unglaciated part of the DEMs as a proxy for the uncertainty of the average elevation change (e.g. Cox et al., 2004). This method corresponds to an extreme case, assuming that the errors of the surface elevation change are totally correlated between all grid cells within the glacier. The opposed extreme case assuming that the errors of surface elevation change are totally uncorrelated between all grid cells has also been applied in the literature (e.g. Thibert et al., 2008). This approach results in an estimated uncertainty reduced by a factor \sqrt{n} compared to the totally correlated uncertainty where n

Geodetic mass balance record with rigorous uncertainty estimates

E. Magnússon et al.

Title Page	
Abstract	Introduction
Conclusions	References
Tables	Figures
◀	▶
◀	▶
Back	Close
Full Screen / Esc	
Printer-friendly Version	
Interactive Discussion	



Geodetic mass balance record with rigorous uncertainty estimates

E. Magnússon et al.

Title Page

Abstract

Introduction

Conclusions

References

Tables

Figures

◀

▶

◀

▶

Back

Close

Full Screen / Esc

Printer-friendly Version

Interactive Discussion



is the number cells for which the difference is calculated. The third alternative, where the spatial dependence of the DEM errors is estimated and inherent in the uncertainty estimate, was described by Rolstad et al. (2009). This method results in uncertainty somewhere between the two extremes and has been adopted in several studies (e.g. Trüssel et al., 2013; Zemp et al., 2013; Fischer et al., 2015). This method includes some simplifications, which so far have not been validated with other geostatistical methods.

Here, we present a case study of Drangajökull ice cap in NW-Iceland (Fig. 1) based on seven sets of aerial photographs in 1946–2005 and a LiDAR DEM obtained from an airplane in 2011 (Jóhannesson et al., 2013). The glacier covered an area of 144 km² in 2011 and is the 5th largest glacier in Iceland. This study describes an alternative method to estimate uncertainties of the average elevation change derived by differencing DEMs, applying geostatistical methods. The approach, which uses the DEM difference from ice and snow free areas as input, allows for a simultaneous estimate of a bias correction for the glaciated part of the DEMs. Both the estimated uncertainty and the bias correction are compared with results from conventional methods. We also interpolate volume changes in areas where data is lacking and inspect how much of the derived volume change may be caused by seasonal variation. The study results in a seasonally corrected mass balance record of Drangajökull ice cap with estimates of possible errors contributing to the record as well as the derived net uncertainty. Finally, we present a simple mass balance model, scaled with the geodetic mass balance results, revealing annual values of glacier-wide winter, summer and net mass balance of Drangajökull in 1958–2011.

2 Data and methods

In this study, seven sets of aerial photographs covering Drangajökull ice cap in 1946, 1960, 1975, 1985, 1986 and 1994 from the archives of the National Land Survey of Iceland, Landmælingar Íslands, and in 2005 from Loftmyndir ehf were used. Negative films were scanned with a photogrammetric scanner in a resolution of 15 and 20 μm.

Geodetic mass balance record with rigorous uncertainty estimates

E. Magnússon et al.

Title Page

Abstract

Introduction

Conclusions

References

Tables

Figures

◀

▶

◀

▶

Back

Close

Full Screen / Esc

Printer-friendly Version

Interactive Discussion



The aerial photographs have an average scale between $\sim 1 : 30\,000$ and $\sim 1 : 40\,000$, which result in a Ground Sampling Distance (GSD) of ~ 0.4 to ~ 1 m. Complete camera calibration information is available for the surveys of 1975, 1985, 1986, 1994 and 2005, but calibration information is lacking for the oldest flights (1946 and 1960). Only the focal length is available for the photographs of 1946, and focal length and radial distortion are available for the photographs of 1960. Table 1 summarizes the main characteristics of each series.

In July 2011 Drangajökull ice cap was surveyed with high resolution airborne LiDAR. The point cloud from the survey was used to produce a high resolution DEM ($2\text{ m} \times 2\text{ m}$ cell size), with an estimated vertical accuracy well within 0.5 m (Jóhannesson et al., 2011). The LiDAR data for Drangajökull was acquired through an effort, initiated during the International Polar Year (IPY) 2007–2009, to produce accurate DEMs of all the major Icelandic glaciers and ice caps (Jóhannesson et al., 2013). The derived DEM covers the entire ice cap as well as the close vicinity of the glacier, which provides a useful reference to constrain and validate other DEMs produced in this study.

2.1 Creation of DEMs and orthorectified photographs

The DEMs were created from the aerial photographs using the software bundle IMAGINE Photogrammetry (© Intergraph). The photogrammetric processing is carried out in four steps: orientation of the images, automatic stereo matching, manual edition of the DEMs and orthorectification of aerial photographs.

Each series of aerial photographs was oriented individually by means of a rigorous bundle adjustment (Wolf and Dewitt, 2010). The glacier is covered by a single series of images for all years except in 1960 when the glacier was covered by three tiles, one per date (Table 1). Tie points were automatically measured in the images and semi-automatically revised, ensuring a good connection between all the adjacent photographs and between strips. The exterior orientation was constrained by using series of Ground Control Points (GCPs) extracted from the LiDAR DEM ($2\text{ m} \times 2\text{ m}$ cell size). The LiDAR DEM was viewed as a hillshade with similar light conditions as during the

acquisition of the photographs. This allowed recognition of and extraction of GCPs from stable features such as boulders and sharp edges in the ice-free areas in the vicinity of the ice cap and at nunataks (Fig. 2). The location of GCPs was based on a regular scheme of distribution surrounding and inside the area of interest in order to ensure stability in the orientation over the entire study area (Kraus, 2007).

The orientation of the 1960 images was carried out using the focal length and lens distortion information obtained from the calibration report of the DMA Cameras (Spriggs, 1966). The 1946 images included information of the focal length written at the margin of the first image of each strip. Both cases needed auxiliary pre-calibration, therefore pseudo-fiducial marks were created allowing the location of a pseudo-principal point (see e.g. Kunz et al. (2012) for details). The orientation of both sets of images included additional parameters in the bundle adjustment for refinement of the camera geometry. Bauer's model (Bauer and Müller, 1972) was used for the images of 1946 and Jacobsen's model (Jacobsen, 1980) was used for the images of 1960.

Once oriented, we produced the elevation point clouds from stereo-matching of the images. The routine eATE (enhanced Automatic Terrain Extraction) of the software allows for a pixel-wise evaluation in the matching process, thus obtaining a high density of points. The low-contrast in firn and snow covered areas caused failures in the matching process. The point clouds for low-contrast areas were therefore created with a configuration based on matching in lower resolution of the images and using larger windows size and lower correlation coefficient. A first edition of the point clouds was carried out with the software CloudCompare (GPL Software); automatic outlier filtering was performed from the PCL plugin "Statistical Outlier Removal" (Rusu et al., 2011) and the dense point clouds were subsampled in regular density of points corresponding to $\sim 10\text{ m} \times 10\text{ m}$ (series of 1960, 1975, 1994 and 2005) or $\sim 20\text{ m} \times 20\text{ m}$ spacing (series of 1946 and 1985), reducing the size of the point clouds and removing double points that could introduce noise when interpolating the point clouds as a grid with fixed cell size (Sects. 2.2 and 2.3). Finally a thorough revision of the results in stereo-

Geodetic mass balance record with rigorous uncertainty estimates

E. Magnússon et al.

Title Page

Abstract

Introduction

Conclusions

References

Tables

Figures



Back

Close

Full Screen / Esc

Printer-friendly Version

Interactive Discussion



scopic vision was carried out, manually editing the DEMs in the glacier areas where the automatic matching failed and surface details were still perceptible.

To delineate the glacier margin and mask out snow covered areas (Sects. 2.2 and 2.4) orthorectified photographs were required. The orthorectification was carried out using preliminary DEMs linearly interpolated from the point clouds as grids with 10 m × 10 m (DEM of 1960, 1975, 1994 and 2005) and 20 m × 20 m cell size (DEM of 1946 and 1985). When monoscopic coverage was only available, the LiDAR DEM was used for the orthorectification, revealing accurately the location of the glacier margin. The orthorectification of all the series of photographs was performed in resolution corresponding to a 2 m × 2 m pixel size.

2.2 DEM error assessment and bias correction

We use the high resolution LiDAR DEM obtained in 2011 to assess the quality of the photogrammetric DEMs. The photogrammetric DEMs are expected to be of significantly worse quality in terms of accuracy than the LiDAR data and we therefore assume for simplicity that statistical parameters derived from the difference between the photogrammetric DEM and the LiDAR DEM (in areas assumed stable) describe errors in the photographic DEM. This is likely to produce a minor underestimate of the actual quality of the photographic DEMs. As described below, all photogrammetric DEMs were bias corrected relative to the LiDAR DEM. A possible bias in the absolute location of the LiDAR DEM does not affect our result since this the bias is cancelled out when calculating the difference between the DEMs.

The first step in estimating the quality of a DEM derived from the aerial photographs was calculating the difference between the photogrammetrically deduced point clouds (Fig. S1 in the Supplement) and LiDAR DEM with 2 m × 2 m cell size. This was calculated using the residual operation in Surfer 12 (©Golden Software, Inc). From this a digital model of the difference between the DEMs was calculated and linearly interpolated within 20 m × 20 m cell size. All cells in the difference model where distance to the next element of the point cloud exceeds 40 m were masked out as well as cells

Geodetic mass balance record with rigorous uncertainty estimates

E. Magnússon et al.

Title Page

Abstract

Introduction

Conclusions

References

Tables

Figures



Back

Close

Full Screen / Esc

Printer-friendly Version

Interactive Discussion



where we expect actual surface changes between the dates of photograph and LiDAR acquisitions. This includes areas which are glaciated and snow covered at either or both dates. The glacier outlines were delineated manually (see Sect. 2.4) and the snow covered areas were derived with semiautomatic classification of the orthorectified aerial photographs and the intensity images derived from the LiDAR scanning. The mean and the standard deviation (σ) of the derived difference (photogrammetric DEM – LiDAR DEM) of the remaining data after snow and glacier masking is tabulated in Table 2.

Extraction of geodetic mass balance requires co-registered DEMs prior to calculation of glacier volume changes. This usually includes estimates of relative vertical and horizontal shift between the DEMs using areas where the elevation change is expected to be insignificant (Kääb, 2005; Nuth and Kääb, 2011; Guðmundsson et al., 2011). In this study the GCPs used during the orientation of the photographs were extracted from the LiDAR DEM in maximum resolution (2 m × 2 m cell size). We were able to extract several GCPs at nunataks near the glacier centre. The distribution of GCPs is therefore fairly regular over the survey area in all cases both spatially (Fig. 2) and with elevation. The orientation of aerial photographs resulted in horizontal RMSE of the GCPs < 3 m in all cases, and typically 1–2 m (Table 2). These values are obtained from least square adjustment resulting in residual mean equal to zero. The horizontal shift relative to the LiDAR DEM is likely to exceed the derived horizontal RMSE locally for a given photogrammetric DEM. It is however very unlikely that the average horizontal shift relative to the LiDAR DEM exceeds the derived RMSE shift of the GCPs. We therefore concluded that horizontal shift corrections are not required for the photographic DEMs.

To compensate for slowly varying errors in the DEM difference the difference in stable areas is commonly used to estimate zero order (bias correction, see e.g. Nuth and Kääb, 2011; Guðmundsson et al., 2011) or higher order correction (e.g. Rolstad, 2009; Nuth and Kääb, 2011). The result from such approach is, however, sensitive to the area chosen as the reference area. One can choose to use the entire area covered by both DEMs outside the glacier or an area limited by a certain distance from the

Geodetic mass balance record with rigorous uncertainty estimates

E. Magnússon et al.

Title Page

Abstract

Introduction

Conclusions

References

Tables

Figures

◀

▶

◀

▶

Back

Close

Full Screen / Esc

Printer-friendly Version





Interactive Discussion



glacier. In this study we apply geo-statistical methods for deriving bias correction of each photogrammetric DEM within the glacier and an estimate of the uncertainty in the derived bias correction. These calculations consisted of five main steps:

- 5 1. Preparation of DEM error input data (derived from the comparison with the LI-DAR), explained below. Resulting error data from ice and snow-free areas is shown in Fig. 3.
2. Calculation of transform function, modifying the input data in such way that its histogram fits normal distribution, with zeros mean and $\sigma = 1$, and transformation of the input data accordingly using the nscore function (Deutsch and Journal, 1998) in WinGSLib V.1.5.8 (© Statios LLC).
- 10 3. Calculation of semivariogram for the nscored input data, but semivariogram describes the variance, γ , of a given coordinate-based variable as a function of distance, d , between sampled locations.
4. Calculation of a spherical variogram model, fitting the derived semivariogram.
- 15 5. Use of the derived spherical model and the nscored data that constrain the semivariogram to run 1000 Sequential Gaussian Simulation (SGSim) of the errors in the glaciated areas using the sgsim function (Deutsch and Journal, 1998) in WinGSLib. The sgsim function includes reversed transformation from the nscored variable to the derived DEM error. SGSim are commonly applied in errors assessments of geo-statistical studies (e.g. Lee et al., 2007; Cardellini et al., 2003). The results from the sgsim runs were used to estimate both the most likely bias of each photogrammetric DEM within the glacier and 95 % confidence level of this bias, as explained further below.

25 The approach adopted here requires that the statistics of the DEM error outside the glacier are descriptive for the errors in the photogrammetric DEM within the glacier margin. This should be kept in mind, both during the photogrammetric processing and

Title Page	
Abstract	Introduction
Conclusions	References
Tables	Figures
	
	
Back	Close
Full Screen / Esc	
Printer-friendly Version	
Interactive Discussion	



Geodetic mass balance record with rigorous uncertainty estimates

E. Magnússon et al.

Title Page

Abstract

Introduction

Conclusions

References

Tables

Figures

◀

▶

◀

▶

Back

Close

Full Screen / Esc

Printer-friendly Version

Interactive Discussion



in the preparation of input data (step 1) used in the geo-statistical calculation. The photogrammetric processing requires fairly even spatial distribution of GCPs, otherwise artificial dip or rise in the photogrammetric DEM are likely to be produced in areas far from a GCP (Kraus, 2007). Such errors would not be represented in a semivariogram based on DEM error in areas where distribution of GCPs is much better. In our case the nunataks of Drangajökull ice cap secure fairly even distribution of GCPs (Fig. 2). The photogrammetric orientations performed in this study never span more than 2 photographs without having constraints from a GCP. This is considered as sufficient coverage of GCPs for a reliable orientation (Kraus, 2007).

The low contrast of snow covered glacier surface may also result in a difference in error statistics between the glacier and the ice and snow free areas (Rolstad et al., 2009). The low contrast should mostly produce high frequency errors, whereas low frequency errors are mostly caused by an inaccurate orientation. The eATE configuration used resulted in fewer but better matching points in the low-contrast areas (Sect. 2.1) and the thorough manual 3-D revision likely removes most of the high frequency noise in the resulting DEM. A semivariogram of the difference between the point cloud in 1946 at low contrast areas and the LiDAR DEM shows variance for $d < 200$ m at similar level as for the data outside the glacier (Fig. 4c). Both cases reveal the dependency of the errors in the 1946 DEM over short distances since variation in elevation changes on the glacier over distances < 200 m are generally small. This supports that the errors in low contrast area unlikely to skew significantly our geo-statistical analyses.

A difference in terrain slope between areas can produce a significant difference in the calculated semivariogram (Rolstad et al., 2009). Local horizontal shift between DEMs can produce significant artificial elevation difference in steep areas. The average slope on the glacier in 2011 was 6.2° whereas the unglaciated area in the 2011 LiDAR DEM had an average slope of 9.8° . The preparation of our data (step 1) therefore includes exclusion of all data where slope exceeds 20° , but unglaciated areas in the 2011 LiDAR DEM, fulfilling this criteria has an average slope of 7.2° .

Geodetic mass balance record with rigorous uncertainty estimates

E. Magnússon et al.

Title Page

Abstract

Introduction

Conclusions

References

Tables

Figures

◀

▶

◀

▶

Back

Close

Full Screen / Esc

Printer-friendly Version

Interactive Discussion



The glaciated parts of the photogrammetric DEMs were all manually revised using 3-D vision, securing removal of significant outliers within the glacier. A thorough revision was not carried out for the unglaciated areas. Instead we apply automatic removal of outliers. This was carried out by calculating standard deviation of the DEM error (photogrammetric DEM- LiDAR DEM), $\sigma_{\varepsilon h}$ (after masking out snow-covered, glacier-covered and steep areas) and filtering the DEM difference with a $500\text{ m} \times 500\text{ m}$ median filter. Values where the difference between the unfiltered and the median filtered value DEM difference exceeded $\sigma_{\varepsilon h}$ were then masked out. The mean DEM error and $\sigma_{\varepsilon h}$ after the slope and outlier masking is shown in Table 2.

The semivariograms obtained with (step 3) and without the nscore transformation of the 1946 DEM error in ice and snow free areas are shown in Fig. 4a and b. The spherical variogram model calculated in step 4 is given as function of d (distance between sampled locations):

$$\begin{aligned} \gamma(d) &= 0 & d &= 0 \\ &= c_0 + c_1 \left[\frac{3d}{2r} - \frac{1}{2} \left(\frac{d}{r} \right)^3 \right] & 0 < d \leq r \\ &= c & d > r \end{aligned} \quad (1)$$

where $c = c_0 + c_1$ and $\gamma(0)$ describes the correlation of a point with itself. The main parameters in the model, nugget (c_0), range (r) and sill (c) are shown in the Fig. 4b. We expect c to equal approximately the global variance of the data set, hence $c \approx 1$ for the nscored data. The shape of the semivariograms that we obtain (Fig. 4a and b and Fig. S2 in the Supplement) indicate a reasonable fitting with a single spherical model unlike in the study by Rolstad et al. (2009) where two spherical models describing the variance at different ranges of distances were required.

The size of the DEM error grid – in full resolution ($20\text{ m} \times 20\text{ m}$ cell size) – was too large for the sgsim function to operate (step 5). The data size was reduced by picking out every 5th column and line in the DEM error grid. In areas where data was sparse,

at nunataks and where few data points remained due the snow mask near the glacier margin, the 20 m × 20 m data was used. Tests with smaller study areas indicated that this reduction of the input data only have minor effects on the results derived from the simulation.

5 Each SGSsim, constrained by the input data and the spherical variogram model and calculated in resolution corresponding to 100 m × 100 m cell size, reveals possible errors in the measured glaciated area of the examined photogrammetric DEM. From each simulation the mean error of the glaciated area was calculated. From the 1000 simulations a histogram was derived and used to approximate a probability function of the
10 likely bias in glaciated part of the DEM. Figure 4f shows the derived histogram for the 1946 DEM. It also shows the mean (Fig. 4d) and γ (Fig. 4e) of the derived error from 1000 simulation at each cell of the simulated area within the glacier. The latter reveals how the uncertainty in the derived error increases with distance from the input data. This should reach a maximum at a distance corresponding approximately to the range
15 (r) in the spherical variogram model, but all points on glacier in the 1946 DEM are at distance $< r$ from input data. The spatially varying mean error (Fig. 4d) could be used directly for correction of the photographic DEM, but instead we subtract the mean of the derived probability function to bias correct the area of interest in the photogrammetric DEM. Both approaches would lead to same result when deducing volume changes
20 from the DEM differencing. The derived bias, z_{bias} , used to correct each DEM, and the corresponding 95 % upper (z_{bias_u}) and lower confidence limits (z_{bias_l}), is tabulated in Table 2. For comparison purposes the table also shows error bars derived by calculating analytically the expected variance ($\sigma_{z_{\text{bias}}}^2$) in the DEM error averaged over circular region corresponding to the size of Drangajökull, using a spherical variogram model (Rolstad et al., 2009), which fits the semivariogram without nscoring the error
25 input data (Fig. 4a).

Geodetic mass balance record with rigorous uncertainty estimates

E. Magnússon et al.

[Title Page](#)[Abstract](#)[Introduction](#)[Conclusions](#)[References](#)[Tables](#)[Figures](#)[◀](#)[▶](#)[◀](#)[▶](#)[Back](#)[Close](#)[Full Screen / Esc](#)[Printer-friendly Version](#)[Interactive Discussion](#)

2.3 Finalizing the glacier DEMs

The photogrammetrically derived point clouds are typically much less dense for the glacier surface than outside the glacier. The typical distance between points on the glacier in the 1946 point cloud (the worst dataset in terms of noise and point density) is ~ 100 m, corresponding approximately to the resolution of the SGSim carried out. The point density is poorer for limited areas and in some regions there are gaps in the point clouds caused by lack of contrast. Interpolating the elevation point clouds directly over long distances can be risky due to the spatial variability of the elevation. The spatial variability of the elevation changes derived from the difference between the point cloud and the LiDAR DEM is expected to be much lower. Therefore the bias corrected difference was interpolated (Sect. 2.2) and added to the LiDAR DEM. The kriging function in Surfer 12 (©Golden Software, Inc.) was used to interpolate the data applying default linear variogram model and data search radius of 500 m. Even though the elevation changes compared to LiDAR are expected to be spatially smooth, interpolation over longer distance would reduce the reliability of the uncertainty assessment carried out for the photographic DEMs. The different interpolation methods used within (kriging) and outside (linear) the glacier produces minor difference in the error statistics. For the 1946 bedrock data (after slope and outlier masking) σ is 4.80 and 4.79 m for the linear and kriging methods respectively but 4.77 m derived directly from the point cloud difference compared to the full resolution LiDAR DEM.

The resulting grids of elevation changes relative to LiDAR contained some larger gaps due to lack of contrast, cloud cover or incomplete coverage of aerial photographs for all datasets except the one of 2005 (Table 2). To complete the difference maps two main interpolation methods were used: for relatively small gaps, spanning short elevation range, kriging interpolation with data search radius > 500 m was applied using the derived elevation difference at the boundary of the data gap as input. For larger areas spanning significant elevation range we estimated a piecewise linear function for the elevation change as function of the 2011 elevation (at 100 m elevation intervals)

Geodetic mass balance record with rigorous uncertainty estimates

E. Magnússon et al.

Title Page

Abstract

Introduction

Conclusions

References

Tables

Figures



Back

Close

Full Screen / Esc

Printer-friendly Version

Interactive Discussion



Geodetic mass balance record with rigorous uncertainty estimates

E. Magnússon et al.

Title Page

Abstract

Introduction

Conclusions

References

Tables

Figures



Back

Close

Full Screen / Esc

Printer-friendly Version

Interactive Discussion



using the elevation difference between the point cloud and the LiDAR DEM as input (see Supplement). For data gaps covering an area at both the east and west side of the glacier the two different interpolations were carried out, one for the area west of the ice divides and another for the area east of it. In four cases neither of the above interpolation methods were considered applicable. The approaches adopted for each of these cases is described in the Supplement. The location of data gaps are shown in Fig. S1 and the interpolation method applied in each case is shown in the Supplement.

The uncertainties associated with interpolation of data gaps in the DEMs was approximated independently from the uncertainties of measured photogrammetric DEMs (Sect. 2.2). It is difficult to quantify these errors, but since these areas are generally small relative to the measured areas we adopted a generous approximation of the uncertainty roughly based on the scatter of the elevation change with altitude (point clouds compared to LiDAR DEMs). We assign three values of elevation uncertainty (95 % confidence level) to the interpolated areas, ± 7.5 , ± 10 and ± 15 m, depending on the quality of the input data used for the interpolation and the applicability of the interpolation method (for further details see Supplement). The interpolated areas with the highest uncertainties were adopted for the lowermost part of Leirufjarðarjökull that was not covered in the 1975 survey flight (see Supplement). Also a relatively large area in southernmost part of Drangajökull in 1946 where the interpolated area is poorly constrained by data. Cluster of nearby data gaps are considered as single area with assigned elevation uncertainty. We however assume that the error in one area is independent from the elevation error in other areas due to the distance between them.

2.4 Delineating glacier margins and nunataks

The glacier margin and nunataks at each time were delineated manually using the orthorectified aerial photographs at given time as well as the derived elevation difference compared to the LiDAR DEM. For 2011 the glacier outlines were drawn based on a shaded relief image of the 2011 DEM in maximum resolution and the intensity image of the LiDAR measurements. All glacier margins were delineated by the same

person. The glacier margin was therefore interpreted in similar manner for all years, in areas where the outlines are uncertain. This working procedure minimizes variations in relative area changes of the ice cap. Due to numerous firn patches in the vicinity of Drangajökull, some of which are connected to the ice cap, it is actually a matter of definition if these connected patches should be included as part of Drangajökull or not. We follow the approach of Jóhannesson et al. (2013) and exclude these patches. In a few areas the aerial photographs do not always reveal the glacier margin. This includes the southernmost part of Drangajökull in 1946. In this area the location of the glacier margin has been very stable since 1960. We therefore adopted at each location, the outermost glacier margin in the 1960–2011 datasets, as the 1946 margin in this area. Data used to approximate the location of the glacier margin in other areas where data is absent is described in the Supplement. The evolution of the glacier area is shown in Fig. 5. Also shown in Fig. 5 is the area of the eastern and western sections of the glacier, when Drangajökull is divided in two along the ice divides from north to south (see Fig. 6).

2.5 Calculating volume changes

To derive the volume change, $\delta V(t_s, t_f)$ of the ice cap during a period $t_s - t_f$, the elevation difference $DEM_f - DEM_s$ (Fig. 6), was integrated over the area covered by glacier at t_s or/and t_f . A continuous DEMs and glacier outlines had been completed for all years except for the year 1994, but this data set covered only $\sim 2/3$ of glacier with the southernmost third of the ice cap missing. In order to estimate volume changes for this part of the glacier in the periods 1985–1994 and 1994–2005 the volume changes for the southernmost third of the glacier were plotted as function of deduced volume changes in the other $\sim 2/3$ of the glacier for the periods 1960–1975, 1975–1985, 1985–2005 and 2005–2011 (Fig. 7). Linear fit describing relation between the volume changes in the two areas estimated with least-squares was used to estimate volume changes for the southern part of the glacier in the period 1985–1994 and 1994–2005. Errors in these volume change estimates were approximated using the 95 % confidence level of

Geodetic mass balance record with rigorous uncertainty estimates

E. Magnússon et al.

Title Page

Abstract

Introduction

Conclusions

References

Tables

Figures



Back

Close

Full Screen / Esc

Printer-friendly Version

Interactive Discussion



the linear fit (estimated in Grapher 10[®] Golden Software, Inc.). Instead of approximat-
ing the position of the 1994 glacier margin, we only approximated the area covered by
this part of the glacier. The volume change for the southernmost part of Drangajökull in
the periods 1975–1985 was approximately the same as the estimated volume change
in 1985–1994. We therefore extrapolate the 0.7 km² area increase of this glacier part
of in 1975–1985 to the period 1985–1994 to estimate the area of this glacier part in
1994.

2.6 Seasonal correction of volume change between DEMs

The DEMs of Drangajökull were extracted from data acquired at different dates dur-
ing the summer or the autumn (Table 1). Deriving mass balance records from DEM
difference without taking this into the account will skew the results, particularly if the
acquisition time of the DEMs differs much from one DEM to another; ideally DEMs at
the start of each glaciological year should be used. In this study the derived volume
change in between DEMs ($\delta V(t_s, t_f)$, in Sect. 2.5) was seasonally corrected by compen-
sating for the expected volume change of the ice cap from the acquisition date of each
DEM until the end of the glaciological year (1 October). The end of the glaciological
year was chosen because it makes comparison with both mass balance records and
meteorological data easier and more eligible. This choice results in larger magnitude of
seasonal correction (and consequently larger uncertainty estimates), when compared to
the average acquisition date of the DEMs. The seasonally corrected volume changes
is given by

$$\delta V^*(t_s, t_f) = \delta V(t_s, t_f) + \delta V_{S_cor}(t_s) - \delta V_{S_cor}(t_f). \quad (2)$$

The expected volume changes, δV_{S_cor} from the time of data acquisitions t_a until the
end of the glaciological year t_{end} was estimated using positive degree day (T_+) model
(e.g. Jóhannesson et al., 1995) with a constant degree day factor (ddf) for the whole
ice cap:

Geodetic mass balance record with rigorous uncertainty estimates

E. Magnússon et al.

Title Page

Abstract

Introduction

Conclusions

References

Tables

Figures

◀

▶

◀

▶

Back

Close

Full Screen / Esc

Printer-friendly Version

Interactive Discussion



Geodetic mass balance record with rigorous uncertainty estimates

E. Magnússon et al.

Title Page

Abstract

Introduction

Conclusions

References

Tables

Figures

◀

▶

◀

▶

Back

Close

Full Screen / Esc

Printer-friendly Version

Interactive Discussion



$$\delta V_{S_cor} = \frac{1}{c_{\delta V_{S_cor}}} \cdot \text{ddf} \sum_{t_a}^{t_{end}} \int_{glacier} T_+(t, x, y) dA \quad (3)$$

where $c_{\delta V_{S_cor}}$ is the conversion factor from the glacier volume change during the period $t_a - t_{end}$ to the melt water draining from the ice cap in the same period. For seasonal volume correction of the 1960, 1975, 1985, 1994, and 2005 DEMs we use daily grids of temperature at 2 m height above ground available for the period 1949–2010 (Crochet and Jóhannesson, 2011). The grids were derived in two steps: (i) applying tension spline interpolation of measured temperature at meteorological stations corrected with fixed lapse rate to represent temperature at sea level. (ii) Lapse rate adjustment of interpolated temperature to compensate for the effects of topography. The temperature grids were in $1 \text{ km} \times 1 \text{ km}$ cell size, but we linearly interpolated the grid in same resolution as the DEMs we are working with ($20 \text{ m} \times 20 \text{ m}$ cell size). The model was scaled to fit the water equivalent of the net glacier volume change (δV) in 1960 to 2005 without any seasonal correction. Assuming that the accumulation/ablation integrated over glacier surface during this time period equals the total winter precipitation/summer melting (P_w/M_s) within the glacier margin we get

$$c_{\delta V} \cdot \delta V(1960, 2005) = P_w(1960, 2005) - M_s(1960, 2005) \quad (4)$$

where

$$P_w(1960, 2005) = \sum_{t_{a1960}}^{t_{a2005}} (1 - S) \int_{glacier(t)} \rho(t, x, y) dA \quad (5)$$

and

$$M_s(1960, 2005) = \text{ddf} \sum_{t_{a1960}}^{t_{a2005}} S \int_{glacier(t)} T_+(t, x, y) dA. \quad (6)$$

Geodetic mass balance record with rigorous uncertainty estimates

E. Magnússon et al.

Title Page

Abstract

Introduction

Conclusions

References

Tables

Figures

◀

▶

◀

▶

Back

Close

Full Screen / Esc

Printer-friendly Version

Interactive Discussion



The conversion factor $c_{\delta V}$ is assumed to be 0.85 (Huss, 2013). p is daily values of precipitation. $S = 1$ from 21 May to 30 September each year, but 0 otherwise, defining the melt season. The definition of summer start is the day of year when the average temperature on the glacier (derived from the interpolated daily temperatures) has on average (in 1949–2010) reached a positive value. At the start of the glaciological year (1 October) this temperature is $\sim 0^\circ\text{C}$. Around 1/3 of 1960 DEM was acquired ~ 3 weeks earlier than the rest (Table 1). The positive degrees in between the two acquisitions were simple given the weight 1/3 (same applies to the 1960 seasonal correction). For area-integration of p and T_+ the glacier area changes stepwise at the mid of each period defined by the DEMs dates.

The daily precipitation data was derived from two sources. The former, referred to as p_1 , was daily precipitation maps (1 km \times 1 km cell size) in 1958–2006 deduced from ERA-40 (Uppala, 2005) by dynamic downscaling with linear model of orographic precipitation (an update of Crochet et al., 2007 described in Jóhannesson et al., 2007). The latter, referred to as p_2 , is daily precipitation maps (1 km \times 1 km cell size) for the period 1991–2012 constructed by combining wind-loss corrected rain-gauge measurements and long-term averaged monthly precipitation maps derived from the LT-model (p_1) through a two step anomaly mapping method (Crochet, 2013). Comparisons made at the Icelandic Meteorological office of the former record with runoff from Hvalá drainage basin near Drangajökull indicated 30–40 % underestimate of precipitation, whereas the latter (p_2) seems fairly representative for the measured runoff. Therefore $p = p_2$ is used for the period 1991–2011 and $p = k \cdot p_1$ for the period 1960–1990, where $k = P_2/P_1$ and P_2 and P_1 represent the total winter precipitation falling on the glacier in the years 1991–2006 (15 winters) integrated from p_2 and p_1 , respectively. This results in $k = 1.30$. If the period is split into the first 8 and last 7 winters, ratios of 1.34 and 1.26 are obtained, indicating rather low variability on decadal time scales.

From Eqs. (4)–(6) a scaled degree day factor $\text{ddf} = 5.4 \text{ mm } ^\circ\text{C}^{-1}$ was obtained. The ddfs calculated by using other periods for scaling are quite consistent. For the periods, 1960–1975, 1975–1985, 1985–1994 and 1994–2005 we get ddf in the range

5.1–5.7 with $0.28 \text{ mm } ^\circ\text{C}^{-1}$ standard deviation. To derive a cautious estimate of the uncertainty in the seasonal correction we assume the variability in ddf is not due to errors in estimated winter precipitation or errors in the deduced volume change but due to Gaussian noise caused by the variability in the degree day factor relating the temperature record and the actual ablation. The standard deviation of ddf for individual years can be formulated as $\sim \sqrt{11} \cdot 0.28 \text{ mm } ^\circ\text{C}^{-1}$ (11 years is the average length of the periods). This multiplied by 1.96 (assuming normal distribution) gives us the 95 % confidence level and therefore $\text{ddf} = 5.4 \pm 1.8 \text{ mm } ^\circ\text{C}^{-1}$. Assuming that our conversion factor $c_{\delta V_{S,\text{cor}}} = 0.75 \pm 0.1$ (where $c_{\delta V_{S,\text{cor}}} = 0.65$ corresponds volume change mostly due to melting of snow and $c_{\delta V_{S,\text{cor}}} = 0.85$ corresponds to volume change mostly due melting of ice) is independent of ddf, results in seasonal corrections from Eq. (3) with 37 % uncertainty (95 % confidence level). The seasonal volume correction of each DEM is shown in Table 3.

The interpolated temperature grids were not available for 2011. Therefore the seasonal correction of the 2011 DEM was instead based on the average daily temperatures at 2 m height above ground in a $3 \text{ km} \times 3 \text{ km}$ grid, extracted from the RÁV-dataset (Rögnvaldsson et al., 2011), which was prepared by dynamically downscaling the operational analysis of the ECMWF with the A-WRF mesoscale atmospheric model (Skamarock et al., 2008). The degree day factor was scaled specifically for these temperature grids, using the period between the DEMs in 2005 and 2011 and the same procedure as described above using the interpolated precipitation maps (Crochet, 2013). The assumed uncertainty in the 2011 seasonal correction corresponds to 37 % of the total correction. The aerial photographs used to produce the 1946 DEM were taken at the beginning of October before the start of winter snow fall. No seasonal correction was therefore required.

Geodetic mass balance record with rigorous uncertainty estimates

E. Magnússon et al.

[Title Page](#)[Abstract](#)[Introduction](#)[Conclusions](#)[References](#)[Tables](#)[Figures](#)[◀](#)[▶](#)[◀](#)[▶](#)[Back](#)[Close](#)[Full Screen / Esc](#)[Printer-friendly Version](#)[Interactive Discussion](#)

2.7 Deriving the geodetic mass balance and its uncertainty

The glacier-wide mass balance rate, \dot{B} (the UNESCO, IACS mass balance terminology (Cogley et al., 2011) is adopted) is estimated during the period $t_s - t_f$, using the equation:

$$5 \quad \dot{B}(t_s, t_f) = \frac{\delta V^*(t_s, t_f)}{\bar{A}(t_s, t_f) \cdot \delta t} c_{\delta V} \quad (7)$$

where $\delta t = t_f - t_s$ and $\bar{A}(t_s, t_f) = (A(t_s) + A(t_f))/2$ approximates the average area of the glacier during the period. It is reasonable to assume that the variables in Eq. (7) are independent of one another, hence the uncertainty in \dot{B} can be approximated as

$$10 \quad \begin{aligned} \Delta \dot{B} &\approx \sqrt{\left(\Delta \delta V^* \frac{\partial \dot{B}}{\partial \delta V^*}\right)^2 + \left(\Delta \bar{A} \frac{\partial \dot{B}}{\partial \bar{A}}\right)^2 + \left(\Delta c_{\delta V} \frac{\partial \dot{B}}{\partial c_{\delta V}}\right)^2} \\ &= \frac{1}{\delta t} \sqrt{\left(\Delta \delta V^* \frac{c_{\delta V}}{\bar{A}}\right)^2 + \left(\Delta \bar{A} \frac{\delta V^* c_{\delta V}}{\bar{A}^2}\right)^2 + \left(\Delta c_{\delta V} \frac{\delta V^*}{\bar{A}}\right)^2}. \end{aligned} \quad (8)$$

$\Delta \bar{A} = 4 \text{ km}^2$ is applied in all cases corresponding to $\sim 2.5\%$ of the glacier area, which is considered a generous estimate of the uncertainty in the glacier area for the given definition (Sect. 2.4). We used $c_{\delta V} = 0.85 \pm 0.06$ (Huss, 2013).

When estimating $\Delta \delta V^*$ the error budget of δV^* was examined. The error, ε , of the seasonally corrected volume change, $\delta V^*(t_s, t_f)$, is the sum:

$$15 \quad \begin{aligned} \varepsilon \{ \delta V^*(t_s, t_f) \} &= \varepsilon \{ V_m(t_s) \} + \varepsilon \{ V_i(t_s) \} + \varepsilon \{ \delta V_{S_cor}(t_s) \} \\ &\quad + \varepsilon \{ V_m(t_f) \} + \varepsilon \{ V_i(t_f) \} + \varepsilon \{ \delta V_{S_cor}(t_f) \} \end{aligned} \quad (9)$$

where the error in the measured volume at time t is

$$\varepsilon \{ V_m(t) \} = A_m(t) \cdot \bar{\varepsilon} \{ h(t) \} \quad (10)$$

where A_m is the area of measured DEM within the glacier and $\bar{\varepsilon}\{h\}$ the mean error of the glaciated area. The error in volume for the interpolated glacier sections lacking measurement (Sect. 2.3) is

$$\varepsilon\{V_j(t)\} = \sum_{j=1}^N A_j(t) \cdot \bar{\varepsilon}\{h_j(t)\} \quad (11)$$

5 where A_j is the area of the interpolated section, j , and $\bar{\varepsilon}\{h_j\}$ is the corresponding mean elevation error. Assuming that the individual errors contributing to Eqs. (9) and (11) are independent of one another the probability function of the error in $\delta V^*(t_s, t_f)$ is given by the multiple convolutions:

$$f_{\varepsilon\{\delta V^*(t_s, t_f)\}} = f_{\varepsilon\{V_m(t_s)\}} \times f_{\varepsilon\{V_i(t_s)\}} \times f_{\varepsilon\{\delta V_{S_{cor}}(t_s)\}} \times f_{\varepsilon\{V_m(t_f)\}} \times f_{\varepsilon\{V_i(t_f)\}} \times f_{\varepsilon\{\delta V_{S_{cor}}(t_f)\}}. \quad (12)$$

10 The probability function $f_{\varepsilon\{V_m(t)\}}$ was derived directly from Eq. (10) and by approximating $f_{\bar{\varepsilon}\{h(t)\}}$ using the histogram of the corresponding elevation bias correction (Sect. 2.2) minus its mean. All other errors are assumed to be normally distributed with zero mean, hence

$$f(\varepsilon) = \frac{1}{\sigma_\varepsilon \sqrt{2\pi}} e^{-\frac{\varepsilon^2}{2\sigma_\varepsilon^2}}. \quad (13)$$

15 The probability distribution $f_{\varepsilon\{V_j\}}$ is hence also a normal distribution with

$$\sigma_{\varepsilon\{V_j\}} = \sqrt{\sum_{j=1}^N (A_j \cdot \sigma_{\bar{\varepsilon}\{h_j\}})^2}. \quad (14)$$

The uncertainty in the volume change $\Delta\delta V$ (95 % confidence level) was now derived from the probability distribution given by Eq. (12). Table 3 shows the 95 % confidence level of $f_{\varepsilon\{V_m\}}$, $f_{\varepsilon\{V_i\}}$ and $f_{\varepsilon\{\delta V_{S_{cor}}\}}$ for each year of acquisition, revealing the main source of error in the derived volume changes.

20

**Geodetic mass
balance record with
rigorous uncertainty
estimates**

E. Magnússon et al.

Title Page

Abstract

Introduction

Conclusions

References

Tables

Figures

◀

▶

◀

▶

Back

Close

Full Screen / Esc

Printer-friendly Version

Interactive Discussion



3 Results

3.1 Bias corrections and uncertainty estimates deduced from the DEM errors

Table 2 gives values of several error estimation parameters the photogrammetric DEMs deduced by comparison with the 2011 LiDAR DEM in ice free areas. Some of these parameters can be used both to correct the DEMs and to estimate the uncertainty of geodetic mass balance results. In some cases significant difference is observed between the mean DEM error, commonly used to correct for bias (0 order correction) of the DEM (e.g. Guðmundsson et al., 2011), and the bias derived from the SGSim. The greatest difference is for the 1946 DEM, which after removal of outliers and steep slopes the ice and snow free part of it has a mean error of -0.86 m whereas the SGSim results in bias of 1.66 m. The difference would presumably be lower if we would only calculate the mean error using areas within certain distance from the glacier margin but it is not straight forward to select this distance without using geostatistical approaches.

The parameters in Table 2 that can be used to estimate the uncertainty of geodetic mass balance show even more diversity. The crudest parameter would be the standard deviation of the DEM error derived from ice and snow free areas. Standard deviation is commonly interpreted as 68 % confidence level assuming normal error distribution and should therefore be multiplied by 1.96 to obtain 95 % confidence level as derived for the other two approaches shown in Table 2. This interpretation of the standard deviation as uncertainty proxy of the volume change implies the assumption that the DEM errors at different locations within the glacier are totally correlated (Rolstad et al., 2009). Since the confidence level of geodetic mass balance results is typically not mentioned in studies using the standard deviation as their uncertainty proxy, the conversion of the standard deviation to 95 % confidence level is omitted in Table 2. The values of standard deviation for the ice free DEMs are 5–45 % lower after removal of outlier and steep slopes. The lower standard deviation values are however still by far higher than the uncertainty (95 % conf. level) of the bias correction derived with SGSim. The SGSim results in uncertainty between 0.21 m (in 2005) and 1.58 m (in 1946). The SGSim un-

certainties correspond to 24–46% of the standard deviation (after slope and outlier removal). If we exclude the three DEMs from 1960, covering only $\sim 1/3$ of Drangajökull each, the range is 24–33%. The SGSim uncertainties correspond to 27–80% of the uncertainties derived with method described by Rolstad et al. (2009) and the percentage seems to depend strongly on the range of the spherical variogram model used in both calculations (Fig. 8).

3.2 DEM seasonal corrections and contribution of different error sources to the geodetic mass balance

The effects of seasonal correction and the estimated contribution of each type of error to the total volume change is summarised in Table 3. The importance of seasonal correction for Drangajökull is clearly revealed, particularly for the first two periods, 1946–1960 and 1960–1975, due to the early acquisition of the 1960 aerial photographs. The sum of the two seasonal corrections for these periods corresponds to larger value than the derived total uncertainty of δV^* . The correction effectively increases the difference in \dot{B} between the periods by $0.35 \text{ m w.e. a}^{-1}$ ($\sim 0.17 \text{ m w.e. a}^{-1}$ absolute change for each period). With the inferred correction the period 1946–1960 is the period of highest loss rate, along with 1994–2005, whereas the period 1960–1975, is only slightly but still significantly negative (Fig. 9). For other periods the net seasonal correction changed the derived \dot{B} by $0.05\text{--}0.08 \text{ m w.e. a}^{-1}$.

The main source of uncertainties is different from one period to another, but in no case is the highest contribution is from the estimated uncertainty of the DEM elevation ($\Delta\delta h_m$ in Table 3). For periods, where volume change is based on the 1946 or 1994 DEM, we have relative high uncertainties due to interpolations of large gaps in the derived DEMs (Fig. 3 and Table 2). The derived value of δV^* for the period 2005–2011, obtained from the best two DEMs in terms of accuracy and coverage, has significant uncertainty due large seasonal correction for both DEMs. The 2005 and 2011 data were acquired in late July, and the summer remainder for both years was relatively

Geodetic mass balance record with rigorous uncertainty estimates

E. Magnússon et al.

Title Page

Abstract

Introduction

Conclusions

References

Tables

Figures

◀

▶

◀

▶

Back

Close

Full Screen / Esc

Printer-friendly Version

Interactive Discussion



warm. The sum of seasonal corrections (which have opposite signs) is actually only half of the uncertainty related to the seasonal corrections for the period 2005–2011.

The uncertainty percentage of δV^* is typically significantly higher than the uncertainty percentage of A (2.5%) and $c_{\delta V}$ ($\sim 7\%$). Uncertainty of the derived \dot{B} (Fig. 9) produced by the uncertainty of the latter two variables is therefore generally minor compared to the uncertainty contribution of δV^*

3.3 The geodetic mass balance of Drangajökull

Figure 9 shows the derived \dot{B} for Drangajökull during six intervals since 1946. During the period 1946–1960 relatively high mass loss rates of $\dot{B} = -0.63 \pm 0.18 \text{ m w.e. a}^{-1}$ are estimated. The mass balance rate was much less negative in 1960–1975 with $\dot{B} = -0.10 \pm 0.08 \text{ m w.e. a}^{-1}$ and was then slightly (but statistically significant) positive in 1975–1994; $\dot{B} = 0.09 \pm 0.08 \text{ m w.e. a}^{-1}$ and $\dot{B} = 0.26 \pm 0.11 \text{ m w.e. a}^{-1}$ in 1975–1985 and 1985–1994, respectively. In the period 1994–2005 again, as in the mid-century, there is high rate of mass loss with $\dot{B} = -0.63 \pm 0.10 \text{ m w.e. a}^{-1}$ and then slightly less negative mass balance rate in 2005–2011, with $\dot{B} = -0.40 \pm 0.14 \text{ m w.e. a}^{-1}$. The glacier wide mass balance rate for the entire period 1946–2011 is $\dot{B} = -0.250 \pm 0.040 \text{ m w.e. a}^{-1}$. In the same period Drangajökull was reduced in area by $\sim 11\%$ from 161 to 144 km² (Fig. 8).

The two lower panels of Fig. 9 show \dot{B} for the western and eastern half of Drangajökull ice cap, as defined by the ice divides from north to south shown in Fig. 6. The results are derived in the same manner as the result for the entire glacier, where the steps taken to correct for bias of the DEM, derive seasonal correction and derive uncertainties were carried out focusing specifically on either the western or the eastern part. The bias correction of each half may vary up to few decimetres from the correction of the entire ice cap and the uncertainty limits of the bias correction is generally slightly higher. By focusing the calculation on each half specifically we also obtain different ddf for the seasonal correction. Assuming the same level of uncertainty as when studying the entire ice cap we derive ddf = $4.9 \pm 1.6 \text{ mm } ^\circ\text{C}^{-1}$ and

Geodetic mass balance record with rigorous uncertainty estimates

E. Magnússon et al.

Title Page

Abstract

Introduction

Conclusions

References

Tables

Figures

⏪

⏩

◀

▶

Back

Close

Full Screen / Esc

Printer-friendly Version

Interactive Discussion



ddf = $6.3 \pm 2.1 \text{ mm } ^\circ\text{C}^{-1}$ for the western and eastern part of Drangajökull, respectively, compared to $ddf = 5.4 \pm 1.8 \text{ mm } ^\circ\text{C}^{-1}$ for the entire ice cap.

Figure 9 shows different evolution of the west and east glacier. Both parts suffered significantly negative mass balance rate in 1946–1960 and 1994–2011. The period in between was significantly negative on the east side, apart from the period 1994–2005, when the upper 95 % confidence level is slightly above 0, whereas the western part had \dot{B} near 0 in 1960–1975 and significantly positive mass balance rate with $\dot{B} = 0.25 \pm 0.10 \text{ m w.e. a}^{-1}$ and $\dot{B} = 0.50 \pm 0.15 \text{ m w.e. a}^{-1}$ in 1975–1985 and 1985–1994, respectively. Mass balance rate of $\dot{B} = -0.136 \pm 0.050 \text{ m w.e. a}^{-1}$ is estimated for the period 1946–2011 on the western part. The mass loss rate is ~3-fold higher for the eastern part with $\dot{B} = -0.376 \pm 0.036 \text{ m w.e. a}^{-1}$. This is also reflected in the area change but in 1946–2011 the eastern part decreased in area 21 %, while the western part shrank only by 3 % (Fig. 8).

3.4 Modelled annual SMB

The method described for deriving the seasonal correction of the volume change results in a routine for estimating \dot{B}_w , \dot{B}_s and \dot{B} on annual bases using the derived ddfs and Eqs. (5) and (6) modified by using time span corresponding to each glaciological year back to 1958 (Fig. 10a; \dot{B}_s extends back to 1949). To validate how this simple model works for deriving B we compare the modelled mass balance rate \dot{B}_{mod} , for each period since 1960, with the derived geodetic results for the same periods (Fig. 9). When looking at the entire ice cap \dot{B}_{mod} (calculated without uncertainties) is within the 95 % confidence limit in 3 of 5 cases but slightly outside the limits in two periods. This indicates a reasonable fit when considering the simplicity of the model. \dot{B}_{mod} obtained for the western and eastern halves of the glacier with the specifically scaled ddfs (Sect. 3.3) is also shown in Fig. 9 for all periods since 1960. \dot{B}_{mod} is generally outside (3 out of 5) or near the 95 % limits of the geodetic results for the western part of the

Geodetic mass balance record with rigorous uncertainty estimates

E. Magnússon et al.

Title Page

Abstract

Introduction

Conclusions

References

Tables

Figures

◀

▶

◀

▶

Back

Close

Full Screen / Esc

Printer-friendly Version

Interactive Discussion



glacier, while on the eastern part \dot{B}_{mod} is within the 95 % confidence level in 4 of the 5 periods.

The model results on annual bases for the entire glacier (Fig. 10a) indicates \dot{B}_{w} generally varying between 2 and 3 m.w.e. a⁻¹ in 1958 to 2011, \dot{B}_{s} between -2 and -4 m.w.e. a⁻¹ and \dot{B} ranging from -1.9 and 1.4 m.w.e. a⁻¹. The model shows that the highest value of \dot{B} observed in 1985–1994 period is partly due to unusually positive mass balance for the glaciological year 1991–92 and 1992–93, when winters of relatively high accumulation were followed by rather cold summers. In 1994–2011 when the geodetic data shows relatively high mass loss rate the annual \dot{B} was probably often near zero or even positive. Most of the mass loss probably occurred during the glaciological years 2002–2003, 2003–2004 and 2009–2010 that according to the model are listed in place 1–3 in terms of negative mass balance for the period 1958–2011.

4 Discussion

The high precision of the geodetic mass balance results presented can be primarily explained by: (i) the use of the high resolution and accuracy LiDAR DEM to extract evenly distributed GCPs for constraining the orientation of photogrammetric DEMs; obtaining equivalent distribution of GCPs in the field was not possible within the financial frame of this study. (ii) The thorough uncertainty assessment of the results where the LiDAR data from ice and snow free areas is also a key data since it enables assessment of geo-statistical parameters of the photogrammetric DEMs. Both (i) and (ii), highlight the need of high resolution and accuracy DEMs from the present in areas of interest to conduct studies of geodetic mass balance using aerial photographs from the past. The third important use of the LiDAR data in this study, is the creation of DEMs from the photogrammetric point clouds within the glacier. Rather than interpolating the elevation point clouds directly we interpolate the difference between the point cloud and LiDAR DEM (much less high frequency variability, the difference is a smoother surface) and

Geodetic mass balance record with rigorous uncertainty estimates

E. Magnússon et al.

Title Page

Abstract

Introduction

Conclusions

References

Tables

Figures

◀

▶

◀

▶

Back

Close

Full Screen / Esc

Printer-friendly Version

Interactive Discussion



DEM error in snow and ice free areas leads to great overestimate of the uncertainty (Table 2). This has been shown before by Rolstad et al. (2009). Other estimators that ignore information of the spatial dependency of the DEM errors, such as the NMAD value (Höhle and Höhle, 2009), should also be considered as incomplete for this purpose.

The difference in uncertainty estimates between the method described here and the method of Rolstad et al. (2009) is especially noteworthy (Table 2 and Fig. 8). Rolstad et al. (2009) provided a simple and logical method to estimate the uncertainty of derived volume change. The DEM errors (or difference) in ice and snow free areas are used to calculate a semi-variogram that constrains a spherical variogram model. From the spherical variogram model alone the expected variance of the DEM error ($\sigma_{z_{bias}}^2$) averaged over circular region corresponding to the size of the glacier is calculated analytically. The method compensate for the spatial dependency of the DEM error at different location within the glacier. The method does however not take into the account how the DEM error within the glacier depends on the DEM errors outside the glacier, unlike the method proposed here utilizing SGSim. This is most likely the explanation why the ratio between the two uncertainty estimates ($\Delta z_{bias_{SGSim}}/\Delta z_{bias_{Rols}}$) appears to be strongly dependent on the range, r , in the spherical variogram model, which is common for both approaches (Fig. 8). If r is small compared the size of the glacier, meaning that large proportion of the glacier has DEM error independent of DEM error outside the glacier, the uncertainty derived SGSim is only slightly smaller than the uncertainty derived analytically from the spherical variogram model alone. If r is however large, meaning that large proportion or even the entire glacier has DEM error dependent on the DEM errors outside the glacier, the SGSim results in much lower uncertainty. This interpretation implies that the method of Rolstad et al. (2009) gives a good approximation of the uncertainty if most of the glaciated area is at distance $> r$ from ice and snow free areas providing measurements of the DEM errors, but can otherwise result in great overestimate of the uncertainty in the derived volume change. The main disadvantage of SGSim approach compared to the approach of Rolstad et al. (2009) is

Geodetic mass balance record with rigorous uncertainty estimates

E. Magnússon et al.

[Title Page](#)[Abstract](#)[Introduction](#)[Conclusions](#)[References](#)[Tables](#)[Figures](#)[⏪](#)[⏩](#)[⏴](#)[⏵](#)[Back](#)[Close](#)[Full Screen / Esc](#)[Printer-friendly Version](#)[Interactive Discussion](#)

that is more time consuming. The tool applied here (WinGSlib) also has problems with dataset larger than worked with in this study. New tools enabling the SGSim approach for large data sets should however be developed in order to facilitate the usage of this methodology.

Our study emphasises the importance of including seasonal correction of DEMs for glacier with high mass turnover to avoid wrong interpretation of derived volume change. The most extreme case is the negative volume change derived from the difference between the 1960 and 1975 DEMs. The seasonal correction results in $\sim 2/3$ of the of this negative volume change being effectively transferred in to the period 1946–1960 due to large seasonal correction of the 1960 DEM resulting from relatively early acquisition of the aerial photographs (Table 1). The seasonally corrected volume change revealing the volume change between the start of different glaciological year obviously has higher uncertainty than the uncorrected volume change. We however consider this trade-off important for easy comparison with other data records, including meteorological data and in situ mass balance measurements. The uncertainty due to the seasonal correction as well as the uncertainty related to the interpolation of the data gaps should be considered as cautious estimates of the 95 % confidence level of the error associated with these two error sources. Effort should be made to constrain these uncertainties further, which could narrow the uncertainty estimates of this study and other similar even further, but it is beyond the scope of this paper.

The presented geodetic mass balance record indicate slower volume decrease for Drangajökull ice cap since the 1940's than for most other glacier in Iceland with geodetic mass balance record extending back to that period. While we observe $\dot{B} = -0.250 \pm 0.040 \text{ m.w.e. a}^{-1}$ for Drangajökull in the period 1946–2011 the corresponding values for Langjökull ice cap in 1945–2011 is $\dot{B} \approx -0.5 \text{ m.w.e. a}^{-1}$ (Fig. 10c). Two outlets of S-Vatnajökull, Kvíárjökull and Skaftárjökull have similar rate of mass decrease in 1945–2010 or $\dot{B} \approx -0.25 \text{ m.w.e. a}^{-1}$ (Hannesdóttir et al., 2015). Other outlets of S-Vatnajökull ice cap show \dot{B}_n between -0.3 and $-0.8 \text{ m.w.e. a}^{-1}$ in 1945–2010 (Hannesdóttir et al., 2015; Aðalgeirsdóttir et al., 2011). For the relatively warm period in

Geodetic mass balance record with rigorous uncertainty estimates

E. Magnússon et al.

[Title Page](#)[Abstract](#)[Introduction](#)[Conclusions](#)[References](#)[Tables](#)[Figures](#)[◀](#)[▶](#)[◀](#)[▶](#)[Back](#)[Close](#)[Full Screen / Esc](#)[Printer-friendly Version](#)[Interactive Discussion](#)

Geodetic mass balance record with rigorous uncertainty estimates

E. Magnússon et al.

Title Page

Abstract

Introduction

Conclusions

References

Tables

Figures

◀

▶

◀

▶

Back

Close

Full Screen / Esc

Printer-friendly Version

Interactive Discussion



1994–2011 we obtain $\dot{B} = -0.552 \pm 0.074 \text{ m.w.e. a}^{-1}$, which is in good agreement with the study of Jóhannesson et al. (2013), which indicated $\dot{B} \approx -0.5 \text{ m.w.e. a}^{-1}$ for Drangajökull ice cap in the period 1996–2011. Comparison of Drangajökull mass balance in 1994–2011, with results from traditional in situ mass balance measurements from Langjökull (in 1996–2011) and Vatnajökull ice caps (Fig. 10a) show that the reduction rate has been $\sim 150\%$ faster on Langjökull ($\dot{B} \approx -1.4 \text{ m.w.e. a}^{-1}$) and $\sim 30\%$ faster on Vatnajökull ($\dot{B} \approx -0.7 \text{ m.w.e. a}^{-1}$).

The difference in the geodetic mass balance results between the east and west part of Drangajökull highlights how difficult it is to extrapolate mass balance records from one glacier to another, even over short distances. The results, showing ~ 3 times more negative mass balance rate for the eastern part of Drangajökull than the western part for the entire period 1946–2011, is not reflected in changing spatial trends of summer temperature during the period. The summer temperature measured east of Drangajökull is typically $\sim 1^\circ\text{C}$ lower than revealed by measurements west of Drangajökull (Fig. 10b) and this is rather consistent throughout the survey period. The precipitation maps do not indicate strong trend in winter accumulation from east to west. The fact that we obtain good fit between geodetic and modelled mass balance records for the eastern part of the ice cap with relatively high ddf but much worse fit for the western part with relatively low ddf could be an indication of an underestimated winter accumulation for western Drangajökull. The explanation for this may be an excess of lee-drying by the LT-model precipitation or transport of snow from east to west by snow drift but the most common wind direction on Drangajökull is from NE. Most of the precipitation also falls on the glacier when the wind blows from NE.

The modelled mass balance record of Drangajökull show annual mass turnover of $\sim 2.5 \text{ m.w.e.}$, significantly higher than at both Vatnajökull and Langjökull ice caps (Fig. 10). If the winter accumulation for western part of Drangajökull is underestimated causing underestimate for the entire ice cap by a factor of 5.4/6.3 (like the difference between ddf for the entire glacier and on the east side might suggest) the annual mass turnover is even higher or $\sim 3 \text{ m.w.e.}$ The modelled record of Drangajökull indicates

Geodetic mass balance record with rigorous uncertainty estimates

E. Magnússon et al.

Title Page

Abstract

Introduction

Conclusions

References

Tables

Figures

◀

▶

◀

▶

Back

Close

Full Screen / Esc

Printer-friendly Version

Interactive Discussion



that the difference in typical year for the positive and negative periods is actually not so great. The difference in the median of annual \dot{B} for the negative period 1975–1994 and the positive period 1994–2011 is only $\sim 0.2 \text{ m.w.e. a}^{-1}$. The main difference between the periods is however caused by few years of extreme mass balance with opposite signs. Figure 10a reveals striking similarities between the modelled \dot{B}_s on Drangajökull and the \dot{B}_s derived with traditional mass balance measurements on Langjökull ice cap, except for the last two years when \dot{B}_s on Langjökull was enhanced by ash fall from the 2010 Eyjafjallajökull eruption and 2011 Grímsvötn eruption. \dot{B}_s on Drangajökull and Langjökull does however correlate much worse with measured on Vatnajökull.

The geodetic mass balance record on Drangajökull ice cap is the first such record revealing glacier volume change in Iceland on decadal time scale the past ~ 70 years. Other records spanning this period have coarser resolution particularly for the period 1945–1985, which is typically assigned a single mass balance value (Fig. 10c). However, accurate and detailed studies pertaining to this period are of particular interest as they may reveal how the Icelandic glaciers responded to the change from a relatively warm climate in 1925–1965 to a significantly colder climate in 1965–1990, and subsequently to a warming with a short setback around 1995 (cf. Figs. 2.6 and 3.1 in Björnsson et al., 2008). We consider this study the first step in filling this gap in our knowledge. The key data to continue this work is the archive of aerial photographs at the National Land Survey of Iceland, covering the Icelandic glaciers in the 1940's–1990's. Similar archives covering other glaciated parts of the world should be fully utilized using the new processing techniques and recent and future availability the of high resolution DEMs of the present state of the glaciated areas and its vicinity.

5 Conclusions

This paper highlights opportunities that new high resolution DEMs are opening to improve the procedure carried out to obtain geodetic mass balance records. We demonstrated how we combine aerial photographs with recent airborne LiDAR data to extract

Geodetic mass balance record with rigorous uncertainty estimates

E. Magnússon et al.

Title Page

Abstract

Introduction

Conclusions

References

Tables

Figures

◀

▶

◀

▶

Back

Close

Full Screen / Esc

Printer-friendly Version

Interactive Discussion



Author contributions. The writing of this paper and the research it describes was mostly carried out by the first two authors of this paper, with inputs from the other three co-authors. All photogrammetric processing and revision of the resulting point clouds was carried out by J. Muñoz-Cobo Belart. The interpolation of the point cloud differences compared to the LiDAR DEM and construction of glacier DEM based on that, interpolation of data gaps, delineation of glacier margin, seasonal correction of the volume change, the construction of the presented mass balance records and associated error analysis was carried out by E. Magnússon based on fruitful discussions with J. Muñoz-Cobo Belart and F. Pálsson. All figures in this paper were made by E. Magnússon and J. Muñoz-Cobo Belart as well as tables. P. Crochet and H. Ágústsson contributed to the handling and interpretation of the meteorological data.

Acknowledgements. This work was carried out within SVALI funded by the Nordic Top-level Research Initiative (TRI) and is SVALI publication number 70. It was also financially supported by alpS GmbH. We thank the National Land Survey of Iceland and Loftmyndir ehf. for acquisition and scanning of the aerial photographs. This study used the recent LiDAR mapping of the glaciers in Iceland that was funded by the Icelandic Research Fund, the Landsvirkjun Research Fund, the Icelandic Road Administration, the Reykjavík Energy Environmental and Energy Research Fund, the Klima- og Luftgruppen (KoL) research fund of the Nordic Council of Ministers, the Vatnajökull National Park, the organization Friends of Vatnajökull, the National Land Survey of Iceland and the Icelandic Meteorological Office. We thank Alexander H. Jarosch for fruitful discussion on the subject of this paper. Auður Agla Óladóttir is thanked for introducing the tools and methodology used in the error analysis of this study to E. Magnússon.

References

- Aðalgeirsdóttir, G., Guðmundsson, S., Björnsson, H., Pálsson, F., Jóhannesson, T., Hannesdóttir, H., Sigurðsson, S. P., and Berthier, E.: Modelling the 20th and 21st century evolution of Hoffellsjökull glacier, SE-Vatnajökull, Iceland, *The Cryosphere*, 5, 961–975, doi:10.5194/tc-5-961-2011, 2011.
- Barrand, N. E., Murray, T., James, T. D., Barr, S. L., and Mills, J. P.: Optimizing photogrammetric DEMs for glacier volume change assessment using laser-scanning derived ground-control points, *J. Glaciol.*, 55, 106–116, 2009.

Geodetic mass balance record with rigorous uncertainty estimates

E. Magnússon et al.

Title Page

Abstract

Introduction

Conclusions

References

Tables

Figures

◀

▶

◀

▶

Back

Close

Full Screen / Esc

Printer-friendly Version

Interactive Discussion



- Bauer, H. and Müller, J.: Height accuracy of blocks and bundle block adjustment with additional parameters, ISPRS 12th Congress, Ottawa, 1972.
- Berthier, E., Schiefer, E., Clarke, G. K. C., Menounos, B., and Remy, F.: Contribution of Alaskan glaciers to sea-level rise derived from satellite imagery, *Nat. Geosci.*, 3, 92–95, doi:10.1038/ngeo737, 2010.
- Berthier, E., Vincent, C., Magnússon, E., Gunnlaugsson, Á. Þ., Pitte, P., Le Meur, E., Masiokas, M., Ruiz, L., Pálsson, F., Belart, J. M. C., and Wagnon, P.: Glacier topography and elevation changes derived from Pleiades sub-meter stereo images, *The Cryosphere*, 8, 2275–2291, doi:10.5194/tc-8-2275-2014, 2014.
- Björnsson, H., Pálsson, F., Guðmundsson, M. T., and Haraldsson, H. H.: Mass balance of western and northern Vatnajökull, Iceland, 1991–1995, *Jökull*, 45, 35–38, 1998.
- Björnsson, H., Sveinbjörnsdóttir, Á. E., Daniélsdóttir, A. K., Snorrason, Á., Sigurðsson, B. D., Sveinbjörnsson, E. Viggósson, G., Sigurjónsson, J., Baldursson, S., Porvaldsdóttir S., and Jónsson, T.: Hnattrænar loftslagsbreytingar og áhrif þeirra á Íslandi – Skýrsla vísindanefndar um loftslagsbreytingar, Umhverfissráðuneytið – The Icelandic Ministry for the Environment and Natural Resources, Reykjavík, Iceland, 118 pp., 2008.
- Björnsson, H., Pálsson, F., Guðmundsson, S., Magnússon, E., Aðalgeirsdóttir, G., Jóhannesson, T., Berthier, E., Sigurðsson, O., and Thorsteinsson, T.: Contribution of Icelandic ice caps to sea level rise: trends and variability since the Little Ice Age, *Geophys. Res. Lett.*, 40, 1–5, doi:10.1002/grl.50278, 2013.
- Cardellini, C., Chiodini, G., and Frondini, F.: Application of stochastic simulation to CO₂ flux from soil: mapping and quantification of gas release, *J. Geophys. Res.*, 108, ECV3–ECV13, 2003.
- Clarke, G. K. C., Jarosch, A. H., Anslow, F. S., Radic, V., and Menounos, B.: Projected deglaciation of western Canada in the twenty-first century, *Nat. Geosci.*, 8, 372–377, 2015.
- Cogley, J. G., Hock, R., Rasmussen, L. A., Arendt, A. A., Bauder, A., Braithwaite, R. J., Jansson, P., Kaser, G., Möller, M., Nicholson, L., and Zemp, M.: Glossary of Glacier Mass Balance and Related Terms, IHP-VII Technical Documents in Hydrology No. 86, IACS Contribution No. 2, UNESCO-IHP, Paris, 2011.
- Cox, L. H. and March, R. S.: Comparison of geodetic and glaciological mass-balance techniques, Gulkana Glacier, Alaska, USA, *J. Glaciol.*, 50, 363–370, 2004.
- Crochet, P.: Gridding daily precipitation with an enhanced two-step spatial interpolation method, Tech. Rep.: PC/2013-01, Icelandic Meteorological Office, Reykjavík, Iceland, 26 pp., 2013.

Geodetic mass balance record with rigorous uncertainty estimates

E. Magnússon et al.

Title Page

Abstract

Introduction

Conclusions

References

Tables

Figures

◀

▶

◀

▶

Back

Close

Full Screen / Esc

Printer-friendly Version

Interactive Discussion



- Crochet, P. and Jóhannesson, T.: A dataset of daily temperature in Iceland for the period 1949–2010, *Jökull*, 61, 1–17, 2011.
- Crochet, P., Jóhannesson, T., Jónsson, T., Sigurðsson, O., Björnsson, H., Pálsson F., and Barstad, I.: Estimating the spatial distribution of precipitation in Iceland using a linear model of orographic precipitation, *J. Hydrometeorol.*, 8, 1285–1306, 2007.
- Deutsch, C. V. and Journel, A. G.: *GSLIB. Geostatistical Software Library and User's Guide*, 2nd Edn., Oxford University Press, Oxford, New York, 369 pp., 1998.
- Fischer, M., Huss, M., and Hoelzle, M.: Surface elevation and mass changes of all Swiss glaciers 1980–2010, *The Cryosphere*, 9, 525–540, doi:10.5194/tc-9-525-2015, 2015.
- Gardelle, J., Berthier, E., and Arnaud, Y.: Slight mass gain of Karakoram glaciers in the early twenty-first century, *Nat. Geosci.*, 5, 322–325, doi:10.1038/NGEO1450, 2012a.
- Guðmundsson, S., Björnsson, H., Magnússon, E., Berthier, E., Pálsson, F., Guðmundsson, M. T., Hognadóttir, T., and Dall, J.: Response of Eyjafjallajökull, Torfajökull and Tindfjallajökull ice caps in Iceland to regional warming, deduced by remote sensing, *Polar Res.*, 30, 72–82, doi:10.3402/polar.v30i0.7282, 2011.
- Hannadóttir, H., Björnsson, H., Pálsson, F., Aðalgeirsdóttir, G., and Guðmundsson, S. V.: Changes in the southeast Vatnajökull ice cap, Iceland, between 1890 and 2010, *The Cryosphere*, 9, 565–585, doi:10.5194/tc-9-565-2015, 2015.
- Höhle, J. and Höhle, M.: Accuracy assessment of digital elevation models by means of robust statistical methods, *ISPRS J. Photogramm.*, 64, 398–406, doi:10.1016/j.isprsjprs.2009.02.003, 2009.
- Huss, M.: Density assumptions for converting geodetic glacier volume change to mass change, *The Cryosphere*, 7, 877–887, doi:10.5194/tc-7-877-2013, 2013.
- Jacobsen, K.: *Vorschläge zur Konzeption und zur Bearbeitung von Bündelblockausgleichungen*, PhD thesis, No. 102, wissenschaftliche Arbeiten der Fachrichtung Vermessungswesen der Universität Hannover, Hannover, 1980.
- James, T. D., Murray, T., Barrand, N. E., Sykes, H. J., Fox, A. J., and King, M. A.: Observations of enhanced thinning in the upper reaches of Svalbard glaciers, *The Cryosphere*, 6, 1369–1381, doi:10.5194/tc-6-1369-2012, 2012.
- Jóhannesson, T., Sigurðsson, O., Laumann, T., and Kennett, M.: Degree-day glacier mass-balance modelling with applications to glaciers in Iceland, Norway and Greenland, *J. Glaciol.*, 41, 345–358, 1995.

Geodetic mass balance record with rigorous uncertainty estimates

E. Magnússon et al.

Title Page

Abstract

Introduction

Conclusions

References

Tables

Figures

◀

▶

◀

▶

Back

Close

Full Screen / Esc

Printer-friendly Version

Interactive Discussion



Jóhannesson, T., Aðalgeirsdóttir, G., Björnsson, H., Crochet, P., Elíasson, E. B., Guðmundsson, S., Jónsdóttir, J. F., Ólafsson, H., Pálsson, F., Rögnvaldsson, Ó., Sigurðsson, O., Snorrason, Á. Sveinsson, Ó. G. B., and Thorsteinsson, T.: Effect of climate change on hydrology and hydro-resources in Iceland, Rep. OS-2007/011, National Energy Authority, Reykjavík, Iceland, 91 pp., 2007.

Jóhannesson, T., Björnsson, H., Pálsson, F., Sigurðsson, O., and Þorsteinsson, Þ.: LiDAR mapping of the Snæfellsjökull ice cap, western Iceland, *Jökull*, 61, 19–32, 2011.

Jóhannesson, T., Björnsson, H., Magnússon, E., Guðmundsson, S., Pálsson, F., Sigurðsson, O., Thorsteinsson, T., and Berthier, E.: Ice-volume changes, bias estimation of mass-balance measurements and changes in subglacial lakes derived by lidar mapping of the surface Icelandic glaciers, *Ann. Glaciol.*, 54, 63–74, doi:10.3189/2013AoG63A422, 2013.

Kääb, A.: Remote Sensing of Mountain Glaciers and Permafrost Creep, Geographisches Institut der Universität Zürich, Zürich, 2005.

Kraus, K.: Photogrammetry – Geometry from Images and Laser Scans, 2nd Edn., de Gruyter, Vienna, Austria, 2007.

Kunz, M., Mills, J. P., Miller, P. E., King, M. A., Fox, A. J., Marsh, S.: Application of surface matching for improved measurements of historic glacier volume change in the Antarctic Peninsula, *Int. Arch. Photogramm. Remote Sens. Spatial Inform. Sci.*, 39, 579–584, 2012.

Lee, S.-Y., Carle, S. F., and Fogg, G. E.: Geologic heterogeneity and a comparison of two geostatistical models; sequential Gaussian and transition probability-based geostatistical simulation, *Adv. Water Resour.*, 30, 1914–1932, doi:10.1016/j.advwatres.2007.03.005, 2007.

Nuth, C. and Kääb, A.: Co-registration and bias corrections of satellite elevation data sets for quantifying glacier thickness change, *The Cryosphere*, 5, 271–290, doi:10.5194/tc-5-271-2011, 2011.

Nuth, C., Kohler, J., Aas, H. F., Brandt, O., and Hagen, J. O.: Glacier geometry and elevation changes on Svalbard (1936–90); a baseline dataset, *Ann. Glaciol.*, 46, 106–116, doi:10.3189/172756407782871440, 2007.

Pálsson, F., Guðmundsson, S., Björnsson, H., Berthier, E., Magnússon, E., Guðmundsson, S., and Haraldsson, H.: Mass and volume changes of Langjökull ice cap, Iceland, ~ 1890 to 2009, deduced from old maps, satellite images and in situ mass balance measurements, *Jökull*, 62, 81–96, 2012.

Geodetic mass balance record with rigorous uncertainty estimates

E. Magnússon et al.

Title Page

Abstract

Introduction

Conclusions

References

Tables

Figures

◀

▶

◀

▶

Back

Close

Full Screen / Esc

Printer-friendly Version

Interactive Discussion



Rögnauldsson, Ó., Ágústsson, H., and Ólafsson, H.: Aflræn niðurkvörðun veðurs innan LOKS verkefnisins (Dynamical downscaling of weather within the LOKS-project), Tech. Rep., Reiknistofa í veðurfræði, Reykjavík, Iceland, 29 pp., 2011.

Rolstad, C., Haug, T., and Denby, B.: Spatially integrated geodetic glacier mass balance and its uncertainty based on geostatistical analysis; application to the western Svartisen ice cap, Norway, *J. Glaciol.*, 55, 666–680, 2009.

Rusu, R. B. and Cousins, S.: 3-D is here: point Cloud Library (PCL), in: Proceedings of the IEEE International Conference on Robotics and Automation (ICRA), May 2011, Shangai, China, 2011.

Skamarock, W. C., Klemp, J. B., Dudhia, J., Gill, D. O., Barker, D. M., Duda, M. G., Huang, X.-Y., Wang, W., and Powers, J. G.: A description of the Advanced Research WRF version 3, Technical Report NCAR/TN-475+STR, National center for Atmosphere Research, Boulder, Colorado, USA, 2008.

Spriggs, R. M.: The calibration of Military Cartographic Cameras, Technical Note, Intelligence and Mapping R. & D. Agency, Wright-Patterson Air Force Base, Ohio, USA, 1966.

Thibert, E., Blanc, R., Vincent, C., and Eckert, N.: Instruments and methods; glaciological and volumetric mass-balance measurements; error analysis over 51 years for Glacier de Sarennes, French Alps, *J. Glaciol.*, 54, 522–532, doi:10.3189/002214308785837093, 2008.

Trüssel, B. L., Motyka, R. J., Truffer, M., and Larsen, C. F.: Rapid thinning of lake-calving Yakutat Glacier and the collapse of the Yakutat Icefield, southeast Alaska, USA, *J. Glaciol.*, 59, 149–161, 2013.

Uppala, S. M., Kallberg, P. W., Simmons, A. J., Andrae, U., Da Costa Bechtold, V., Fiorino, M., Gibson, J. K., Haseler, J., Hernandez, A., Kelly, G. A., Li, X., Onogi, K., Saarinen, S., Sokka, N., Allan, R. P., Andersson, E., Arpe, K., Balmaseda, M. A., Beljaars, A. C. M., Van De Berg, L., Bidlot, J., Bormann, N., Caires, S., Chevallier, F., Dethof, A., Dragosavac, M., Fuentes, M., Hagemann, S., Holm, E., Hoskins, B. J., Isaksen, I., Janssen, P. A. E. M., Jenne, R., McNally, A. P., Mahfouf, J. F., Morcrette, J. J., Rayner, N. A., Saunders, R. W., Simon, P., Sterl, A., Trenberth, K. E., Untch, A., Vasiljevic, D., Viterbo, P., and Woollen, J.: The ERA-40 re-analysis, *Q. J. Roy. Meteorol. Soc.*, 131, 2961–3012, 2005.

Vaughan, D. G., Comiso, J. C., Allison, I., Carrasco, J., Kaser, G., Kwok, R., Mote, P., Murray, T., Paul, F., Ren, J., Rignot, E., Solomina, O., Steffen, K., and Zhang, T.: Observations: cryosphere, in: *Climate Change 2013: The Physical Science Basis. Contribution of Working Group I to the Fifth Assessment Report of the Intergovernmental Panel on Climate Change,*

edited by: Stocker, T. F., Qin, D., Plattner, G.-K., Tignor, M., Allen, S. K., Boschung, J., Nauels, A., Xia, Y., Bex, V., and Midgley, P. M., Cambridge University Press, Cambridge, UK and New York, NY, USA, 317–382, 2013.

5 Wolf, P. and Dewitt, B. A.: Elements of Photogrammetry; with Applications in GIS, McCraw Hill, Boston, MA, USA, 2000.

Zemp, M., Thibert, E., Huss, M., Stumm, D., Rolstad Denby, C., Nuth, C., Nussbaumer, S. U., Moholdt, G., Mercer, A., Mayer, C., Joerg, P. C., Jansson, P., Hynek, B., Fischer, A., Escher-Vetter, H., Elvehøy, H., and Andreassen, L. M.: Reanalysing glacier mass balance measurement series, The Cryosphere, 7, 1227–1245, doi:10.5194/tc-7-1227-2013, 2013.

TCD

9, 4733–4785, 2015

**Geodetic mass
balance record with
rigorous uncertainty
estimates**

E. Magnússon et al.

Title Page

Abstract

Introduction

Conclusions

References

Tables

Figures



Back

Close

Full Screen / Esc

Printer-friendly Version

Interactive Discussion



**Geodetic mass
balance record with
rigorous uncertainty
estimates**

E. Magnússon et al.

Title Page

Abstract

Introduction

Conclusions

References

Tables

Figures

◀

▶

◀

▶

Back

Close

Full Screen / Esc

Printer-friendly Version

Interactive Discussion

**Table 1.** Dates, main parameters and notes describing the data sets used in the study.

Date	N. Images	Average GSD* (m)	Notes
12 Oct 1946	15	0.94	Missing southernmost part of Drangajökull. Over-exposed areas
Summer 1960	40	0.42	Divided in 3 flights: 14 Jun 1960, 08 Jul 1960 and 12 Jul 1960.
5 Sep 1975	18	0.77	Missing Leirufjarðarjökull outlet.
27 Jul 1985	32	0.70	Missing Reykjarfjarðarjökull outlet.
4 Aug 1986	5	0.70	Used for filling the gaps of 1985 on Reykjarfjarðarjökull outlet
29 Aug 1994	21	0.53	Missing southern part
27 Jul 2005	57	0.53	Complete coverage
20 Jul 2011	–	–	Complete coverage (LiDAR)

* GSD: Ground Sampling Distance.

Geodetic mass balance record with rigorous uncertainty estimates

E. Magnússon et al.

Table 2. The horizontal RMSE of the GCPs (nr. of GCPs within brackets), glacier coverage and error assessment of the photogrammetric DEMs, using four different approaches: (i) Direct comparisons of ice-free areas (mean and standard deviation). (ii) Comparisons in ice-free areas after masking out outliers and areas with slope $> 20^\circ$ (see Sect. 2.2). (iii) SGSim. z_bias corresponds the mean elevation bias from 1000 simulation, z_bias_u and z_bias_l the upper and lower 95 % confidence level and $\Delta z_bias = (z_bias_u - z_bias_l)/2$. (iv) Method described by Rolstad et al. (2009). To derive uncertainties with 95 % conf. level we assume normal probability function and therefore $\Delta z_bias_{Rols} = 1.96 \times \sigma_{z_bias_Rols}$.

Year	RMSE XY GCPs (m)	Glacier cover- age (%)	Error mean ice-free (m)	SD ice- free (m)	Error mean ice- free masked (m)	SD ice-free masked (m)	z_bias (m)	z_bias_l (m)	z_bias_u (m)	Δz_bias (m)	Δz_bias_{Rols} (m)
1946	2.99 [43]	75.3	-0.95	5.09	-0.86	4.80	1.66	0.12	3.27	1.58	3.41
1960 W	2.87 [25]	31.0	0.37	2.23	0.49	1.84	0.48	-0.34	1.34	0.84	1.05
1960 C	2.54 [31]	30.5	-0.31	2.08	-0.26	1.52	0.34	-0.29	1.02	0.66	1.04
1960 E	2.21 [47]	35.6	0.03	2.26	0.09	1.51	0.20	-0.45	0.93	0.69	0.96
1975	1.22 [44]	96.5	0.48	2.05	0.39	1.52	0.03	-0.47	0.48	0.48	0.62
1985	1.37 [33]	87.2	-0.67	1.97	-0.60	1.15	-0.48	-0.80	-0.17	0.32	0.47
1994	0.84 [40]	66.3	-0.09	1.04	-0.09	0.80	0.22	-0.03	0.47	0.25	0.72
2005	1.14 [55]	100.0	-0.24	1.30	-0.26	0.87	0.22	0.01	0.42	0.21	0.78

[Title Page](#)
[Abstract](#)
[Introduction](#)
[Conclusions](#)
[References](#)
[Tables](#)
[Figures](#)

[Back](#)
[Close](#)
[Full Screen / Esc](#)
[Printer-friendly Version](#)
[Interactive Discussion](#)


Geodetic mass balance record with rigorous uncertainty estimates

E. Magnússon et al.

Table 3. The average elevation change during periods defined by the DEMs before and after the seasonal correction, the seasonal correction corresponding to DEM at time t_s and t_f (the correction at t_f is shown with minus sign since this correction term has minus in front of it in Eq. 2), the uncertainties (95 % conf. level) of seasonally corrected elevation change and the uncertainty contribution from the seasonal corrections, DEM errors and interpolation of data gaps, respectively All values were originally calculated in terms of volumes but are here averaged over the area $\bar{A} = (A(t_f) + A(t_s))/2$.

t_s	t_f	Average δh (m)	Average δh^* (m)	Average $\delta h_{S_cor}(t_s)$ (m)	Average $-\delta h_{S_cor}(t_f)$ (m)	Average $\Delta \delta h^*$ (m)	Average $\Delta \delta h_{S_cor}$ (m)	Average $\Delta \delta h_m$ (m)	Average $\Delta \delta h_s$ (m)
1946	1960	-7.36	-10.31	0	-2.95	2.74	1.09	1.28	2.19
1960	1975	-4.73	-1.84	3.08	-0.18	1.33	1.14	0.62	0.39
1975	1985	2.06	1.06	0.19	-1.18	0.96	0.44	0.54	0.62
1985	1994	2.15	2.73	1.19	-0.61	1.15	0.49	0.32	1.08
1994	2005	-7.11	-8.09	0.62	-1.60	1.17	0.63	0.26	0.96
2005	2011	-2.38	-2.83	1.62	-2.07	0.99	0.97	0.21	0

Title Page

Abstract

Introduction

Conclusions

References

Tables

Figures

◀

▶

◀

▶

Back

Close

Full Screen / Esc

Printer-friendly Version

Interactive Discussion



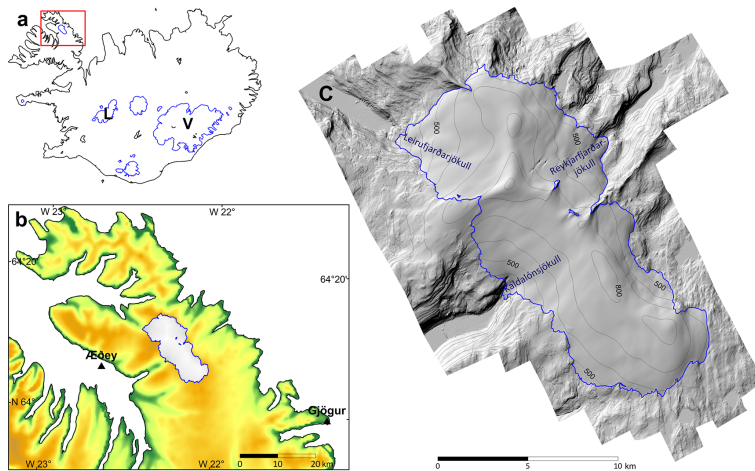


Figure 1. Location of study area. Blue lines in (a) are the outline of the larger glaciated areas in Iceland and the letters L and V indicates the location of Langjökull and Vatnajökull ice caps, respectively. The triangles in (b) indicates the locations of the meteorological stations at Æðey and Gjögur. Image (c) shows a Lidar DEM of Drangajökull (glacier margin shown with blue line) and vicinity obtained in 2011 (Jóhannesson et al., 2013) represented as shaded relief image and contour map (100 m contour interval). The names and locations of the 3 main outlet glaciers are shown.

Geodetic mass balance record with rigorous uncertainty estimates

E. Magnússon et al.

Title Page	
Abstract	Introduction
Conclusions	References
Tables	Figures
◀	▶
◀	▶
Back	Close
Full Screen / Esc	
Printer-friendly Version	
Interactive Discussion	



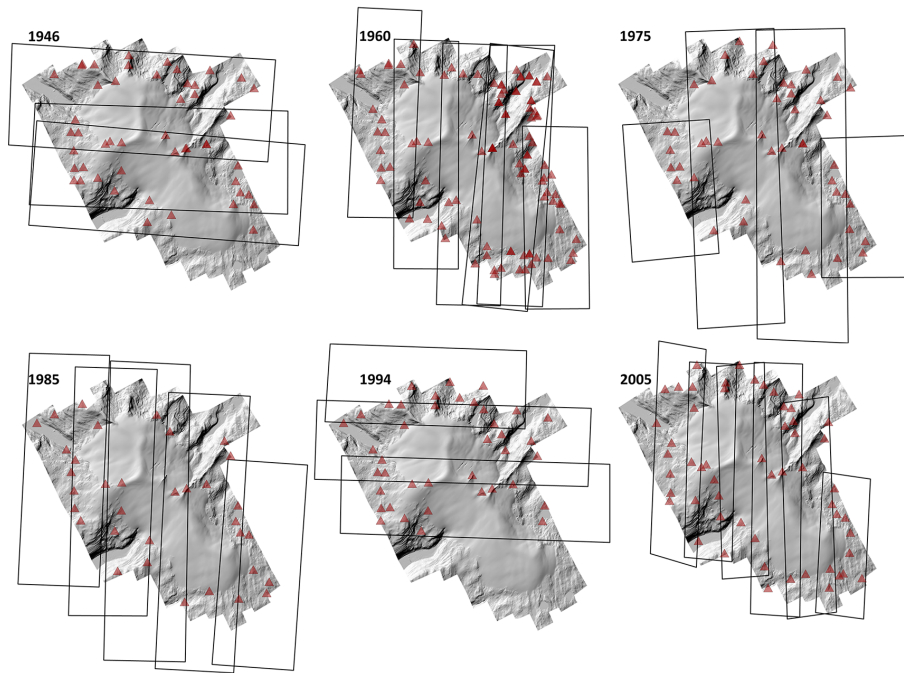


Figure 2. The coverage of aerial photographs at different epochs with the LiDAR DEM as background. The GCPs used for orientation of each series of aerial photographs are marked with triangles.

**Geodetic mass
balance record with
rigorous uncertainty
estimates**

E. Magnússon et al.

Title Page	
Abstract	Introduction
Conclusions	References
Tables	Figures
◀	▶
◀	▶
Back	Close
Full Screen / Esc	
Printer-friendly Version	
Interactive Discussion	



Geodetic mass balance record with rigorous uncertainty estimates

E. Magnússon et al.

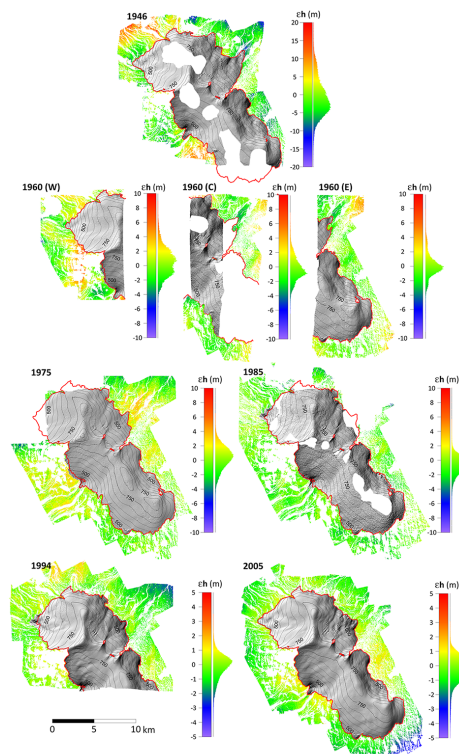


Figure 3. The series of DEMs of Drangajökull ice cap created from the aerial photographs. The shaded relief images and contour maps indicate the glaciated part of each DEM. The derived elevation errors in the vicinity of the glacier (after masking out outliers and areas with slope $> 20^\circ$) are shown as color images. The color scale is extended for the DEM in 1946 and reduced for the 1994 and 2005 DEMs. A vertical histogram next to the scale bar shows the error distribution.

[Title Page](#)[Abstract](#)[Introduction](#)[Conclusions](#)[References](#)[Tables](#)[Figures](#)[◀](#)[▶](#)[◀](#)[▶](#)[Back](#)[Close](#)[Full Screen / Esc](#)[Printer-friendly Version](#)[Interactive Discussion](#)

Geodetic mass balance record with rigorous uncertainty estimates

E. Magnússon et al.

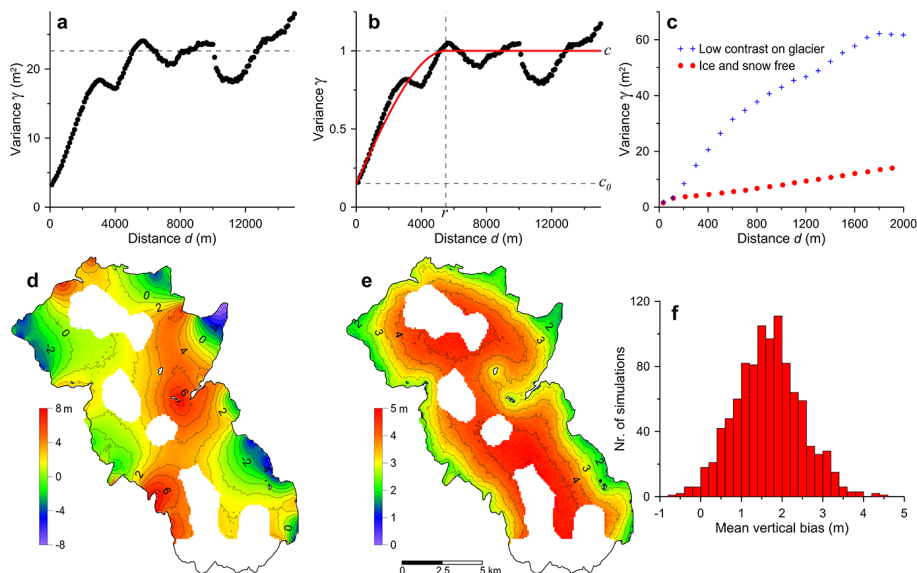


Figure 4. The variograms of the 1946 DEM error before **(a)** and after **(b)** nscoring the data. The DEM error data is derived from the elevation difference compared to the LiDAR DEM in ice and snow free areas. Outliers in the elevation difference and areas with slope $> 20^\circ$ were also masked out. The spherical variogram model (red line) used in the SGSim and the parameters defining it (c , c_0 and r) are shown in **(b)**. **(c)** shows comparison between variograms for the deduced error (same as in **a**) and the difference compared to the LiDAR DEM in low contrast areas within the glacier. **(d)–(f)** shows the results of the SGSim for the 1946 DEM. **(d)** and **(e)**, respectively show the mean and standard deviation of 1000 simulations at each $100\text{ m} \times 100\text{ m}$ pixel. Graph **(f)** shows histogram (0.2 m bins) of the mean vertical bias values deduced from each simulation.

Title Page

Abstract

Introduction

Conclusions

References

Tables

Figures

◀

▶

◀

▶

Back

Close

Full Screen / Esc

Printer-friendly Version

Interactive Discussion

Geodetic mass balance record with rigorous uncertainty estimates

E. Magnússon et al.

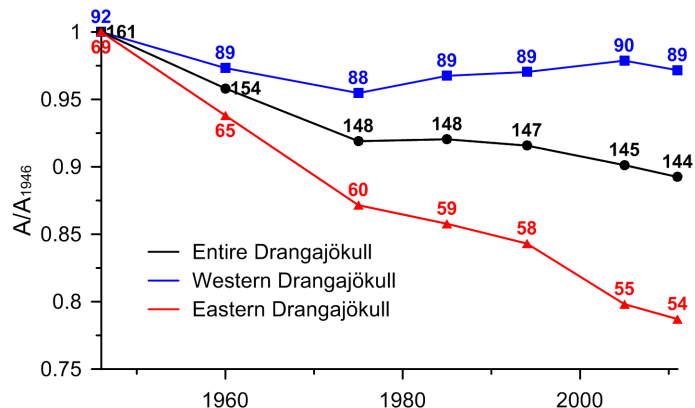
[Title Page](#)
[Abstract](#)
[Introduction](#)
[Conclusions](#)
[References](#)
[Tables](#)
[Figures](#)
[Back](#)
[Close](#)
[Full Screen / Esc](#)
[Printer-friendly Version](#)
[Interactive Discussion](#)


Figure 5. The relative area change of all, the western and the eastern sections of Drangajökull ice cap (relative to the initial area in 1946). The purple lines in Fig. 6 show the ice divides; they are used to define the east and west sections of the glacier. Labels give the glacier area in km^2 at each epoch.

Geodetic mass balance record with rigorous uncertainty estimates

E. Magnússon et al.

Title Page

Abstract

Introduction

Conclusions

References

Tables

Figures

◀

▶

◀

▶

Back

Close

Full Screen / Esc

Printer-friendly Version

Interactive Discussion

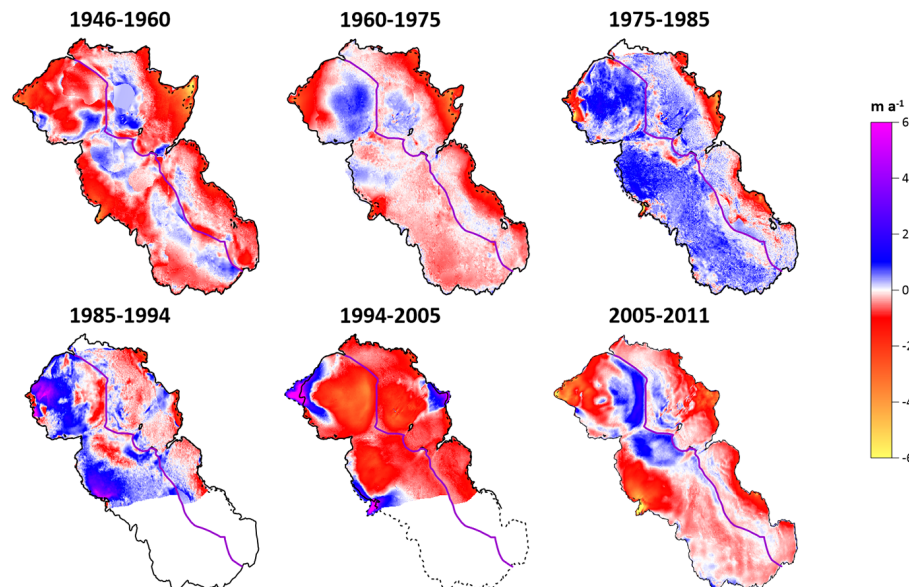


Figure 6. The average annual elevation change of Drangajökull during 6 intervals since 1946. Red colors indicate thinning and blue colors thickening.

Geodetic mass balance record with rigorous uncertainty estimates

E. Magnússon et al.

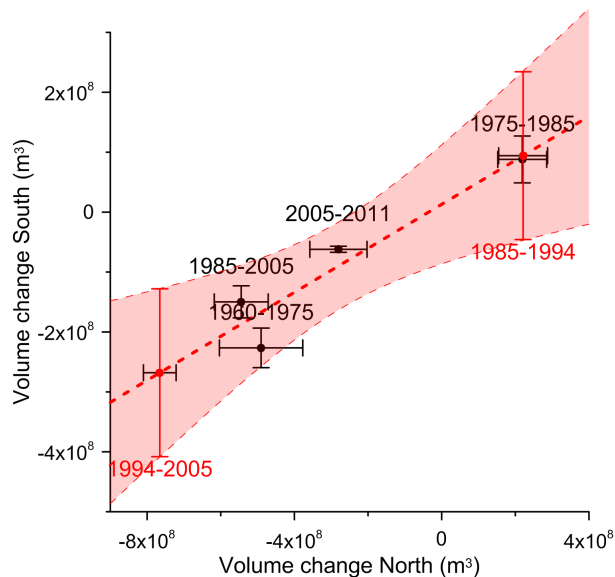


Figure 7. The volume change of the southernmost of Drangajökull, which is missing in the 1994 DEM (Fig. 3), plotted as function of the volume change in the area north of it covered by the 1994 DEM, for the periods available (shown with black labels). The thick dashed line shows linear fit for the data points with the 95% confidence area shown as light red. The red dots are the corresponding volume change estimates for the southern part in 1985–1994 and 1994–2005.

[Title Page](#)
[Abstract](#)
[Introduction](#)
[Conclusions](#)
[References](#)
[Tables](#)
[Figures](#)
[◀](#)
[▶](#)
[◀](#)
[▶](#)
[Back](#)
[Close](#)
[Full Screen / Esc](#)
[Printer-friendly Version](#)
[Interactive Discussion](#)


Geodetic mass balance record with rigorous uncertainty estimates

E. Magnússon et al.

Title Page

Abstract

Introduction

Conclusions

References

Tables

Figures

◀

▶

◀

▶

Back

Close

Full Screen / Esc

Printer-friendly Version

Interactive Discussion

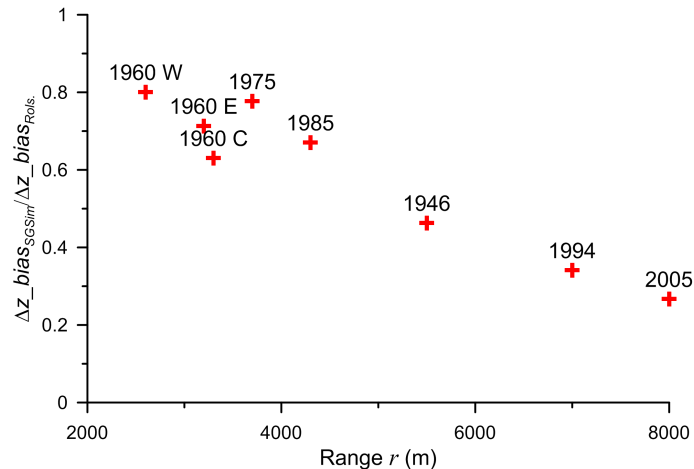


Figure 8. The ratio between uncertainties (95 % conf. level) from the methods demonstrated in this work and the method demonstrated by Rolstad et al. (2009) as function of the range, r , in the deduced spherical variogram model. The DEM epoch corresponding to each point is shown with a label.

Geodetic mass balance record with rigorous uncertainty estimates

E. Magnússon et al.

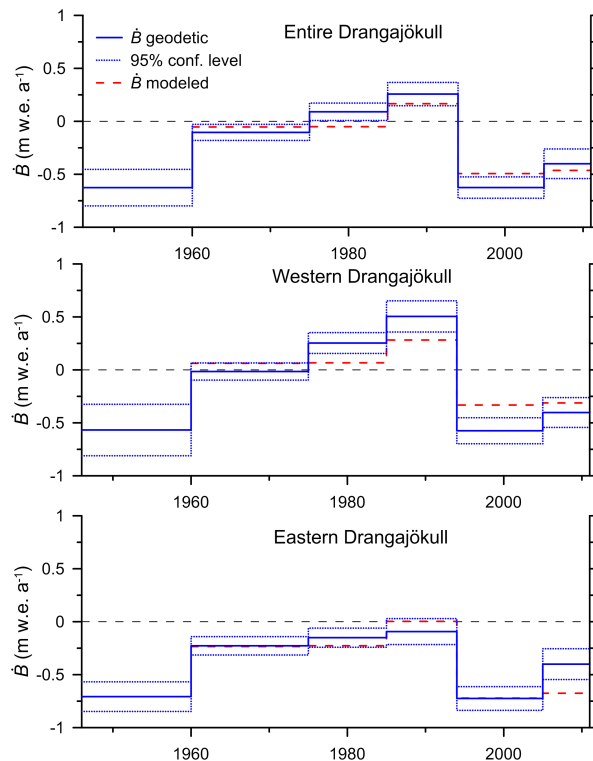


Figure 9. The glacier-wide mass balance rate (\dot{B}) of all, the western and the eastern sections of Drangajökull ice cap during 6 different periods since 1946, derived with geodetic methods (blue line). The purple lines in Fig. 6 show the ice divides used to splitting the ice cap between the east and west sections. The dashed red line shows the glacier-wide mass balance rate for the same periods estimated from mass balance model (see Sect. 2.6 and Fig. 10).

Title Page

Abstract

Introduction

Conclusions

References

Tables

Figures

◀

▶

◀

▶

Back

Close

Full Screen / Esc

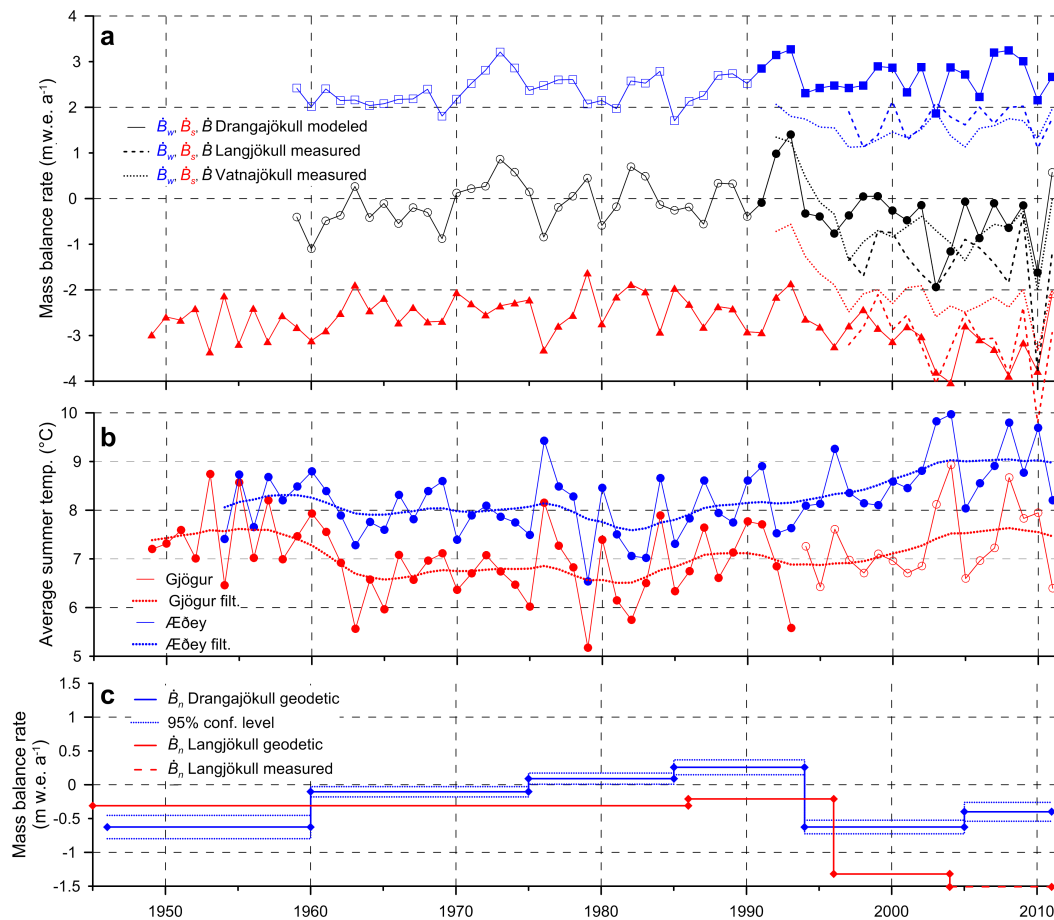
Printer-friendly Version

Interactive Discussion



Geodetic mass balance record with rigorous uncertainty estimates

E. Magnússon et al.



Title Page

Abstract

Introduction

Conclusions

References

Tables

Figures

◀

▶

◀

▶

Back

Close

Full Screen / Esc

Printer-friendly Version

Interactive Discussion



Figure 10. (a) The modeled glacier-wide mass balance rate (summer, winter and net) of Drangajökull (solid lines). Closed blue boxes denote annual values \dot{B}_w derived by integrating in space and during given winter daily precipitation maps interpolated from bias corrected rain-gauge measurements (Crochet, 2013). Open blue boxes, denotes \dot{B}_w derived using daily precipitation maps downscaled from ERA-40 (an update of Crochet et al., 2007 described in Jóhannesson et al., 2007), multiplied with a scaling factor (see Sect. 2.6). The closed red triangles show B_s derived with degree day model using the daily grids of interpolated temperature at 2 m height above ground (Crochet and Jóhannesson, 2011) available in 1949–2010. The open triangle in 2011 is derived using temperature at 2 m height from Rögnvaldsson et al. (2011) and ddf scaled for the period 2005–2011 (see Sect. 2.6). The dash and dot line shows for comparison measured values of \dot{B}_w , \dot{B}_s and \dot{B} for Langjökull and Vatnajökull ice caps, respectively (Björnsson et al., 1998, 2013). **(b)** The average summer temperature at the meteorological stations Gjögur, since 1949, and Æðey since 1954 (see Fig. 1b, for locations). Close circles indicate data from manned station, open circles from automatic station. The dot lines show the average summer temperature at each location filtered with 11 year triangular filter. **(c)** The geodetic results of \dot{B} for Drangajökull ice cap, compared with geodetic observations from Langjökull ice cap (Pálsson et al., 2012). The record is extended to 2011 for Langjökull with traditional mass balance measurements shown in **(a)**. See Fig. 1a for locations.

Geodetic mass balance record with rigorous uncertainty estimates

E. Magnússon et al.

Title Page	
Abstract	Introduction
Conclusions	References
Tables	Figures
◀	▶
◀	▶
Back	Close
Full Screen / Esc	
Printer-friendly Version	
Interactive Discussion	

